

Integration of calibration and alignment procedures for the reconstruction of muons in the ATLAS experiment

Diplomarbeit der Fakultät für Physik

der

Ludwig-Maximilians-Universität München



vorgelegt von

Matthias Obermaier

28. Januar 2005

Erstgutachterin: Prof. Dr. Dorothee Schaile

Zweitgutachter: Prof. Dr. Wolfgang Dünneberger

Abstract

The ATLAS experiment, together with the Large Hadron Collider, starts taking data in 2007. Monitored Drift tube (MDT) chambers will constitute the large majority of precision detectors in the Muon Spectrometer, which is part of the ATLAS detector. A fraction of these MDT chambers are commissioned and calibrated at the Munich Cosmic Ray Measurement Facility. This is achieved by utilizing muons originating from cosmic ray reactions passing the MDT chamber setup. Track reconstruction of these muons is performed by the MuonCosmicTeststand (MCT) software package. The software collection is based on the ATLAS software framework and integrates simulation, detector description, conditions data and reconstruction. Muon trajectories reconstructed by the MCT package are used to determine wire positions within the MDT chambers.

In this thesis, an alternative way of chamber alignment within the MCT package was introduced and different procedures were tested and implemented in order to take subtle effects into account, which caused small biases before. Additionally, further techniques were developed in order to categorize systematic deviations from the nominal MDT chamber geometry. The algorithms include calculation of intrinsic geometry distortions on different levels: Aside from global alignment parameters, further parameters can be determined on multilayer and single-layer level, as well as parameters concerning twisted chamber ends and tubespacing effects.

Contents

Abstract	5
1 Introduction	9
1.1 The ATLAS detector	9
1.2 Importance of muons in high energy physics	11
1.2.1 Search for Higgs particles	11
1.2.2 SUSY search	12
1.2.3 B Physics	13
1.3 Muon chambers and Testing	14
1.3.1 ATLAS muon chambers	14
1.3.2 The Munich Cosmic Ray Measurement Facility	15
2 MCT - a pilot project in the ATLAS Software Framework	17
2.1 Athena Overview	17
2.1.1 Athena Basics	17
2.1.2 ATLAS Software framework concepts	18
2.1.3 Athena-specific approaches	19
2.2 MCT overview	22
2.2.1 Simulation in the MCT package	22
2.2.2 Track reconstruction using the MCT package	22
2.2.3 MCT calibration issues	24
3 Chamber alignment and wire position analysis	27
3.1 Alignment	27
3.1.1 Original chamber alignment	27
3.1.2 Introducing a new alignment procedure	32
3.1.3 Fit optimization in the alignment processes	33
3.2 Determination of wire displacements	36
3.2.1 Determination of wire position deviations in the test chamber	36
3.2.2 Test chamber alignment on analysis level	37
4 Classification of MDT alignment parameters and their determination	39
4.1 MDT elements to be treated as rigid bodies	40
4.1.1 Global alignment on analysis level	40
4.1.2 Multilayer misalignment and tilts	40
4.1.3 Single-layer misalignment and tilts	42
4.2 Non-rigid-body chamber deformations	42

4.2.1	Twisted chamber ends	42
4.2.2	Tube-spacing	44
4.2.3	Remaining wire displacements	45
5	Results	47
5.1	Comparison: MCT alignment and wire position analysis to tomograph data	47
5.2	Results for alignment parameters	53
6	Summary	57
A	Description of a MCT reconstruction job	59
B	Implementation of the new wire positions analysis	63

Chapter 1

Introduction

The Standard Model in high-energy physics provides an accurate description of elementary particles and fundamental interactions. However, different effects and predictions within or beyond the Standard Model remain to be validated. The ATLAS¹ detector is designed to maximize the discovery potential for new physics and therefore, precise calibration of the detector components is of vital importance.

1.1 The ATLAS detector

In 1994, the CERN² council decided, along with various supporting governments worldwide, to build a new particle accelerator, the LHC³ within the existing LEP⁴ tunnel at the research facility near Geneva, Switzerland. The aim of this new accelerator is to raise the energy region that is experimentally accessible by nearly one order of magnitude: The LHC will accelerate protons in the 27km ring to 7 TeV, thus providing a center-of-mass-energy of 14 TeV for two colliding proton beams. The former upper limit of 1.96 TeV center-of-mass-energy was given by the TeVatron, located at the FNAL⁵.

Given that one of the main goals of the LHC is to observe new physics, new frontiers have to be crossed in detector technology, as higher beam energies require increasing material effort. In one of LHC's interaction points, notably the one which lies adjacent to the CERN research facilities, the ATLAS detector is being constructed. Assembled in a huge cavern, the detector measures a total of 44 m in length and 22 m in diameter, weighing approximately 7000 t when completed.

As shown in figure 1.1, the inner detector, placed directly around the interaction point, is surrounded by a solenoidal magnetic field at 2 T and measures 7 m in length and 1.15 m in diameter. The purpose of the inner detector is recognition of charged particle tracks and momentum and vertex measurements. This will be achieved by high-resolution, semiconducting pixel and strip detectors in the innermost part of the tracking volume. These detector elements allow the determination of primary

¹A Toroidal LHC ApparatuS

²Centre Européenne pour la Recherche Nucléaire

³Large Hadron Collider

⁴Large Electron Positron collider

⁵Fermi National Accelerator Laboratory, Chicago

and secondary particle reaction vertexes to a high level of precision. The outer part consists of continuous straw-tube tracking detectors which are also capable of performing transition radiation detection.

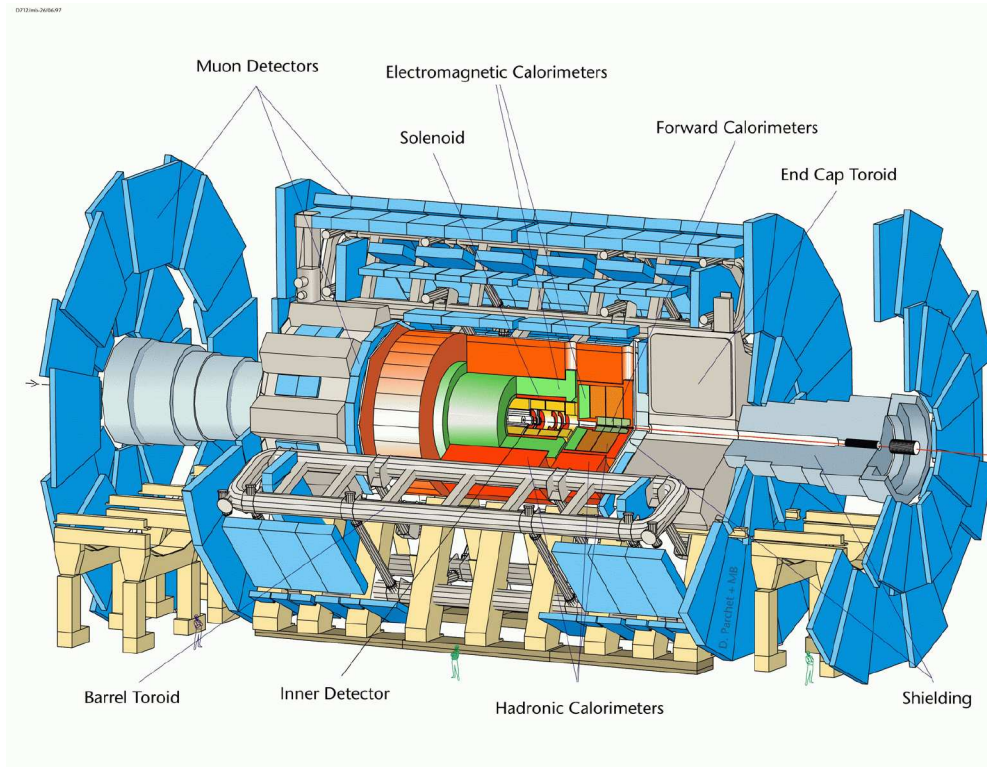


Figure 1.1: Outline of the ATLAS detector (from inside to outside): tracker, calorimeter and muon system. The beam pipe is located along the symmetry axis with the interaction point in the center of the setup.

Liquid-argon (LAr) electromagnetic calorimeters with a high granularity cover a pseudo-rapidity range of $|\eta| < 3.2$. Excellent performance in terms of energy and position resolution is expected here, as well as in the end-cap detectors, which consist of the hadronic calorimeters and the electromagnetic end-cap calorimetry detectors, sharing the same cryostats. These cryostats also house the LAr forward calorimeters which extend the pseudo-rapidity range to $|\eta| = 4.9$. The major part of hadronic calorimetry is performed by a scintillator-tile calorimeter, which is divided into a large barrel and two smaller end-cap cylinders which are located on each side of the barrel. The calorimeter design is expected to provide especially good performance for jet and missing-energy detection.

The muon spectrometer contributes mainly to the huge size of the ATLAS detector. Multiple muon chambers are arranged in a way that a muon, emerging from the interaction point, has to cross at least three muon chambers. The center of the ATLAS detector is entirely surrounded by a barrel-shaped muon chamber system (see figure 1.2). Different sizes of muon chambers are assembled (Barrel Inner Small, Barrel

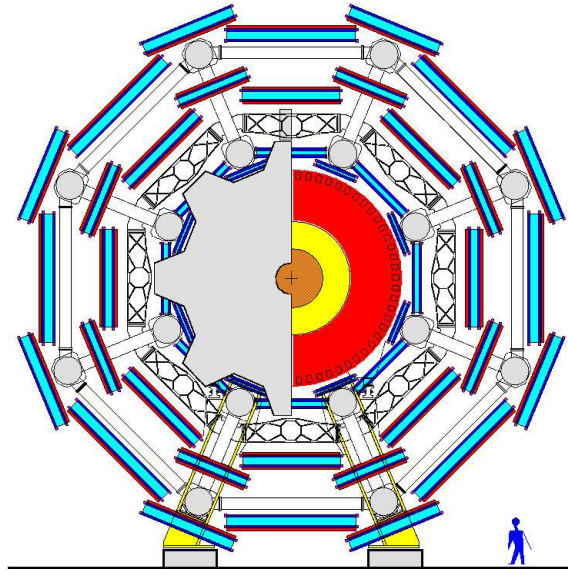


Figure 1.2: Cross section of the ATLAS detector. The muon system encloses the inner detector in a barrel-like manner.

Inner Large, Barrel Middle Small, Barrel Middle Large, Barrel Outer Small and Barrel Outer Large) in this barrel geometry, while additional end-cap stations cover the open spots in the barrel geometry, providing a full 4π - coverage. The other component of the muon spectrometer is the air core toroid system. There are three sub-components: one barrel toroid and two end-cap toroids to fit with the muon chamber system. They provide a magnetic field, which averages about $0.6 T$ and causes a deflection of muon trajectories. Together with the light and open structure of the air-core toroid system, which is designed to reduce multiple-scattering effects, precise muon momentum measurements becomes possible.

The ATLAS detector as a whole is designed to operate at very high luminosities (at about $10^{34} \text{ cm}^{-2} \text{ s}^{-1}$). Aside from detector hardware issues, this also sets enormous challenges concerning trigger design and computing. On the one hand, a sophisticated trigger design is essential to reduce the amount of events to be recorded from 40 MHz to about 100 Hz , while, on the other hand, a data volume of about 2 Peta-bytes per year has to be processed and stored, together with 1 Peta-byte of simulation data (see chapter 2).

1.2 Importance of muons in high energy physics

1.2.1 Search for Higgs particles

One of the main goals of the ATLAS experiment is the search for the Higgs particle, which is supposed to be the explanation for spontaneous symmetry breaking in electroweak theory.

The Standard Model in particle physics refers to a total number of 6 leptons and 18 quarks (3×6 quarks for each color charge). Together with their antiparticles, this sums

up to 48 fermions, that is, spin-1/2 - particles. The spin-1 - particles, also known as bosons, are: γ , W^\pm , Z^0 and g . All of these elementary⁶ particles have been experimentally observed in the past.

However, there is one issue that remains to be resolved. The Standard Model gives no answer to how particles actually get their mass and why there are such non-intuitive differences in the masses of e.g. photons and Z-Bosons. Therefore, the Higgs-Mechanism was introduced, which led to the prediction of a further particle that should be observable, namely the Higgs boson. This theory describes the existence of an omnipresent, yet undiscovered field, the Higgs Field, for which the Higgs bosons are the field quanta. The different particles gain their masses by interacting with the Higgs field. Theoretical considerations and experimental results suggest that the Higgs boson is expected in the mass range between 114 GeV and 1 TeV , if it exists. Depending on the Higgs mass, there are different decay channels for the Higgs boson that are kinematically possible. Some of them are particularly important for detection in ATLAS because of their clear signature. These are:

$$\begin{aligned}
 H &\longrightarrow \gamma\gamma ; m_H < 150 \text{ GeV} \\
 H &\longrightarrow ZZ^* \longrightarrow 4l^\pm ; 130 \text{ GeV} < m_H < 182 \text{ GeV} \\
 H &\longrightarrow WW \longrightarrow l^\pm \nu 2 \text{ Jets}, 2l^\pm 2\nu ; m_H > 161 \text{ GeV} \\
 H &\longrightarrow ZZ \longrightarrow 4l^\pm, 2l^\pm 2\nu, 2l^\pm 2 \text{ Jets} ; m_H > 182 \text{ GeV}
 \end{aligned}$$

The mass range below 182 GeV , which is $2 \cdot m_Z$, doesn't allow the production of 2 real Z bosons, while no pairs of real W bosons can be produced in the mass range below 161 GeV ($2 \cdot m_W$). The ATLAS detector with its common, onion-skin design, where each detector layer encloses the preceding one, is designed to be able to provide a highly precise reconstruction of these collision events. Due to the presence of leptonic decay products in Higgs events, in particular for the Higgs boson decaying into vector boson pairs, it is especially important to have a well designed, built and calibrated muon spectrometer in order to do accurate muon tracking.

1.2.2 SUSY search

The presence of the Higgs particle as a single, elementary scalar boson implicates further problems, notably when regarding radiative corrections to the Higgs mass. Therefore, some theorists suggest that there is a more general description of particles and their interactions, called supersymmetry, which features particles at TeV -mass scale yet to be discovered. The concept of providing symmetry to fermions and bosons should lead to a unified description of fundamental interactions. The theories of supersymmetry try to relate bosons and fermions, as well as to introduce gravity into theories of particle interactions. Supersymmetric models postulate the existence of *super-partners* for all particles that are presently observed. There are bosonic super-partners for fermions (squarks and sleptons) and fermionic super-partners of bosons (gluinos and gauginos). Further postulates are the existence of multiple Higgs bosons. A large set of particles with different masses, couplings and decay modes can be derived thereof, where the specific parameters remain to be measured. The theory predicts that supersymmetric particles are not heavier than a few TeV .

⁶as it is considered today

If super-symmetric particles actually exist, they obviously don't have the same masses as their standard model counterparts - otherwise, they would have been detected a long time ago. The LHC and the ATLAS detector are designed to provide beam energies sufficiently high to break into the mass regions of super-symmetric particles and to get experimental proof for super-symmetric theories.

Minimal Super-gravity (mSUGRA) is a less general, but more predictive model which expresses masses, couplings and branching ratios of super-symmetric particles in terms of only a few parameters. A promising candidate for detection is the trilepton channel, deriving from a neutralino ($\tilde{\chi}_2^0$) decay. The decay mode

$$q\bar{q} \longrightarrow W^* \longrightarrow \tilde{\chi}_1^\pm \tilde{\chi}_2^0$$

produces three leptons, which can be detected in the ATLAS muon system, and a neutrino. A precise muon spectrometer is essential to do high-performance missing-energy calculations which are required by the above channel.

1.2.3 B Physics

Assuming perfect symmetry in the world of elementary particles, the moment of origin of our universe should have produced as many antiparticles as there were particles. This would, however, have led to complete matter-anti-matter-annihilation. But obviously, there is some matter left which hasn't been annihilated by antimatter. An explanation for this fact is the charge conjugation (charge and parity, CP) violation. Experiments in the latter half of the 20th century show that CP symmetry is not universally valid, but can be violated in certain cases. Neutral kaon decays are reactions which feature CP violation, but the origin of this effect has not yet been fully understood.

CP violation can be observed in B-meson decays, where some deeper understanding of the origins is expected. The ATLAS detector is especially suitable for B physics, because of its flexible trigger setup, improved inner detector technologies and a high-performance muon system to allow missing-energy calculations and lepton identification to great accuracy.

$$\begin{aligned} B_d^0 &\longrightarrow J/\Psi K_S^0 \\ B_d^0 &\longrightarrow \pi^+ \pi^- \end{aligned}$$

are decay modes where CP violation can be observed. LHC's total $b\bar{b}$ cross section is rather high, at about 1/100 of the total LHC cross section. Therefore, enough data will be produced for deeper investigations on those decay modes that are rather rare elsewhere. Even more rare decay modes like

$$B_{s,d}^0 \longrightarrow \mu^+ \mu^- (X)$$

are expected to be observed.

1.3 Muon chambers and Testing

1.3.1 ATLAS muon chambers

The Monitored Drift Tube chambers (MDT chamber, see figure 1.3) in ATLAS consist of aluminium tubes of 30.035 mm in diameter. Each tube contains a $50\ \mu\text{m}$ Wolfram wire, strained in the center of the tube. This wire represents the anode for ionization measurements, the cathode being the tube wall (which has a thickness of 0.39 mm).

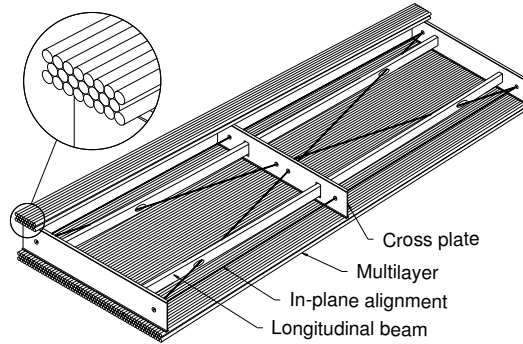


Figure 1.3: Schematic view of a Monitored Drift Tube Chamber, as used in ATLAS.

The ATLAS BOS (Barrel Outer Small) chambers, which are to be commissioned and calibrated in Munich, are arranged in layers of 72 tubes each, leaving no space between them. These layers are grouped in multilayers, consisting of three layers. Each layer is displaced by half a tube diameter with respect to the previous layer before being glued into place, see the insert in figure 1.3. Thus, the distance between the center of the tubes in the direction perpendicular to the layer plane is given by

$$\Delta z = \sqrt{(2r_t + d_g)^2 - r_t^2}$$

where Δz is the vertical center-to-center distance, r_t is the (outer) drift tube radius and d_g is the thickness of the gluing layer. The multilayers are further arranged in groups of two multilayers, which are mounted on an aluminium suspension consisting of longitudinal beams and cross plates. The suspension structure separates the two multilayers by a distance of approx. 400 mm , measured from multilayer center to multilayer center.

Means to determine deviations of the nominal chamber positions and small distortions in chamber geometry are provided by the RasNiK system [10]. Optical and capacitive alignment systems monitor the chamber geometry complementary to alignment procedures which utilize cosmic ray muons (see chapters 3 and 4). However, in the ATLAS experiment, the RasNiK system is crucial for the MDT chamber alignment, since muons produced in LHC collisions are of limited use for the alignment, due to the restricted angular range.

This construction now forms an MDT chamber of the ATLAS BOS type, with total dimensions of $4.0\text{ m} \times 2.2\text{ m} \times 0.5\text{ m}$. 88 BOS chambers are currently being assembled

by the MPI⁷ in Munich. Each chamber is then transported to Garching to be equipped with electronics.

1.3.2 The Munich Cosmic Ray Measurement Facility

The MDT chambers delivered by the Munich MPI are commissioned and calibrated within the Munich Cosmic Ray Measurement Facility in Garching. Each drift tube is filled with the reaction gas, a mixture of $ArCO_2$ in a 93 : 7 ratio, the same medium that is to be used in the actual ATLAS detector. After gas leakage tests have been performed, each chamber is inserted into the measurement facility, which is depicted in figure 1.4.

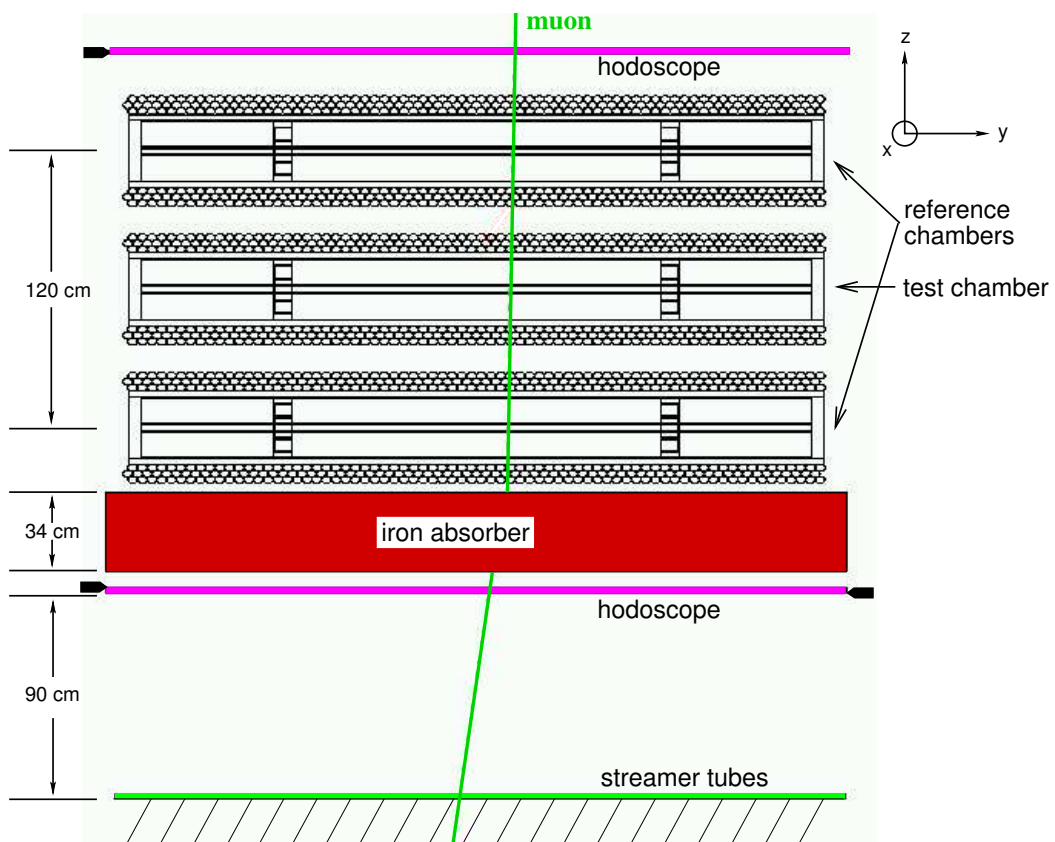


Figure 1.4: Schematic view of the Cosmic Ray Measurement Facility

For the local measurement procedures, a right-handed coordinate system is defined [13], with the x coordinate collinear along the wires. The y coordinate is defined in the layer plane, perpendicular to the x - axis, while the z - axis is defined perpendicularly to the layer plane, pointing upwards.

Asides from suspension structures, the outermost parts of the measurement facility are the hodoscopes. The upper hodoscope is a single scintillator layer while the lower

⁷Max-Planck-Institut

hodoscope consists of two scintillator layers which are displaced with respect to each other. This hodoscope configuration delivers trigger functionality within the cosmic ray measurement setup. Together with a 34 cm iron absorber layer, which is intended to filter out muon momenta below 600 MeV, the upper and lower hodoscopes trigger signals caused by a single muon passing through the measurement facility. Muons showing a significant inclination to the x-z- plane are omitted, due to the trigger configuration of 5 segments in x - direction.

The hodoscopes, consisting of scintillator bars, are also capable of performing muon track measurements along the x coordinate. The resolution is, however, limited to (8 cm) there. This hodoscope configuration triggers muon events at a rate of approximately 70 Hz.

The hodoscopes and the iron absorber enclose two muon chambers, operating as *reference chambers*, which in turn encompass a third MDT chamber, the *test chamber*. The reference chambers were calibrated using the X-ray tomograph at CERN; therefore, their wire positions are well known. The test chamber is the actual test item, with its wire position deviations from the nominal chamber geometry yet to determine.

The MDT chambers in the measurement facility record hit data caused by muons passing through the setup. The recorded muons originate almost exclusively from cosmic ray reactions in the upper atmosphere. Data obtained by recording hit information can be used to reconstruct track information for the reference chambers as well as for the test chamber. Track information can now be compared event by event, whereas systematic deviations between local tracks provided by the test chamber and those obtained from the reference chambers are used to calculate wire position deviations for the drift tubes of the test chamber. To gain a sufficiently good result for wire displacement measurements, high statistics is needed. The test chambers inserted at the Munich Cosmic Ray Measurement Facility are typically left under measuring conditions for at least 32 hours, producing several millions of muon events. The measurement facility is equipped with an air conditioning system which confines day/night temperature differences to a maximum of about 1 Kelvin. Considering the thermal expansion coefficient of aluminium of

$$\lambda = 23.1 \cdot 10^{-6} \frac{1}{K}$$

this leads to a maximum thermal deviation of $\approx 50 \mu m$ in y direction. However, air temperature is not the only effect, as there can be direct sunlight on the setup during daytime.

Chapter 2

MCT - a pilot project in the ATLAS Software Framework

In August 2002, development started on the MuonCosmicTeststand (MCT) package, a muon simulation and reconstruction package for the ATLAS software framework. This software collection is designed specifically for the Munich Cosmic Ray Measurement Facility.

The ATLAS software framework, commonly referred to as Athena, provides powerful tools for simulation, detector description, reconstruction and handling of calibration data. The MCT package aims to utilize these to perform simulation and reconstruction at the measurement facility, in order to test and apply the tools and to gain experience with Athena.

The MCT Package is not the only approach to fulfill the task of track reconstruction and wire positions analysis. The existing software solution in Munich, which is in productional use, is the MTOffline Package (see [16], [17]), exclusively developed in Garching. This software allows high-precision wire position measurements, though it does not make use of the ATLAS software framework due to the development status of Athena at that time.

Based on the approach to use cosmic muons crossing the drift tube chamber for wire position measurements, the MCT package works just as MTOffline. A complete processing cycle has been modeled and developed in the MCT package. Starting from raw data, the package is capable to perform software-based chamber calibration for the measurement facility, as well as to simulate and reconstruct muon trajectories for further wire position analyses.

2.1 Athena Overview

2.1.1 Athena Basics

Athena is the main ATLAS software framework, designed to be capable of fulfilling all ATLAS reconstruction and simulation tasks. Based on the Gaudi [4] framework, which is used in several high-energy-physics experiments, the Athena framework is completely written in C++ and relies exclusively on object-oriented programming

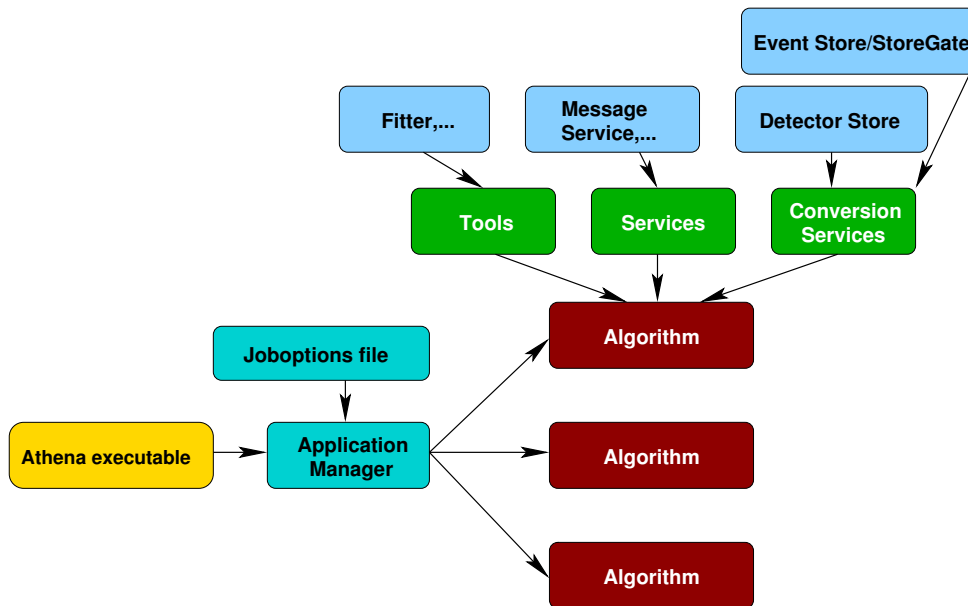


Figure 2.1: Layout of the Athena concept. Starting from the Athena executable, a variety of framework components can be used and specified via joboptions

techniques. Reconstruction and simulation processes can change over time, and an object-oriented approach facilitates changing, replacing and re-using certain elements of code. Considering the size of the ATLAS project, a lot of software developers contribute to the ATLAS software framework. Object-oriented programming helps to divide programming and implementation tasks to get a largely complete and working reconstruction and simulation tool. Even more important is that the Athena framework is mostly independent from any underlying changes that may occur. For example, different operating systems, as well as database systems may be appropriate to use, and therefore, an additional layer of abstraction is introduced and the actual access to storage techniques is completely separated from the algorithms by converters.

The Athena framework makes use of the so-called *joboptions concept* (see figure 2.1). By starting an Athena job, the user specifies a *joboptions file* to be read by the Athena application manager which is, in fact, the only service called in the Athena executable. The joboptions file utilizes the python programming language and allows a user to start certain Athena framework functionality and to modify different parameters interactively. This is very useful when running Athena since it avoids "hard-wired" parameter code.

2.1.2 ATLAS Software framework concepts

In the Athena framework, several base classes are defined, which user-specific algorithms can derive from. They provide different run-time objects. Firstly, there is a base class called `Algorithm`. This base class provides functionality to process data in the way, particle physicists are most familiar to, namely when a large number of "events" is to be processed, one after another. For this, the `Algorithm` base class mainly con-

sists of three abstract functions, which have to be implemented and overloaded (and can then be called by the framework):

- `initialize()` - is executed once, at the beginning of a data processing job. Different data-acquisition tools are called here and parameter values, specified in joboptions, are set.
- `execute()` - is called once for each event. The actual algorithm, i.e. calculations that have to be done for each event, is included here.
- `finalize()` - is the function called after the `execute()` - cycle, but only once. Some post-event-cycle - operations can be included, such as summary calculations and statistic printouts.

Different algorithms can be instantiated in parallel, by means of the store-gate-mechanism (2.1.3). The actual order of `execute()` - function calls in the different algorithms can also be defined in the joboptions file.

The next type in the Athena framework is the `Tool` base class. Tool classes are meant to be invoked by other Athena components and can be used to implement algorithms which are to be re-used at several other places in Athena. Once implemented, these classes follow the philosophy of object-oriented programming languages and can be reused in the entire framework. Track fitters are examples for classes implemented by inheriting from the `Tool` base class, which can be quickly interchanged in that way. Another type of functionality in the Athena framework is provided by Services. Services can again be used in the entire framework and are instantiated only once. One example for a service is `ToolSvc`, which acts as an interface to the actual tools, as every Athena component needs to interact with `ToolSvc` when requesting a tool. The message service `MsgSvc` is another example of a service which, in this case, provides Athena-wide standard-output steering functionality.

One of the most important Athena base classes are the `Converters` and `ConversionServices`, which are an essential part of the framework. They maintain the independence of production algorithms from specific storage technologies. Storage technology may be distinguished as

- *transient storage*, which is the in-memory data representation and
- *persistent storage*, the permanent data storage, like tape libraries or hard disks.

There are two `ConversionSvcs`, one for each storage type, and further `Converters`, which actually convert data from existing storage technologies. Communication between `ConversionSvcs` and `Converters` provides the desired technology-independent functionality for Athena algorithms.

2.1.3 Athena-specific approaches

As mentioned in chapter 2.1.1, the joboptions concept is an approach which is special to Athena because it separates Athena from being a static application. Libraries are dynamically specified and loaded at run time, unlike standard Linux/Unix library sharing.

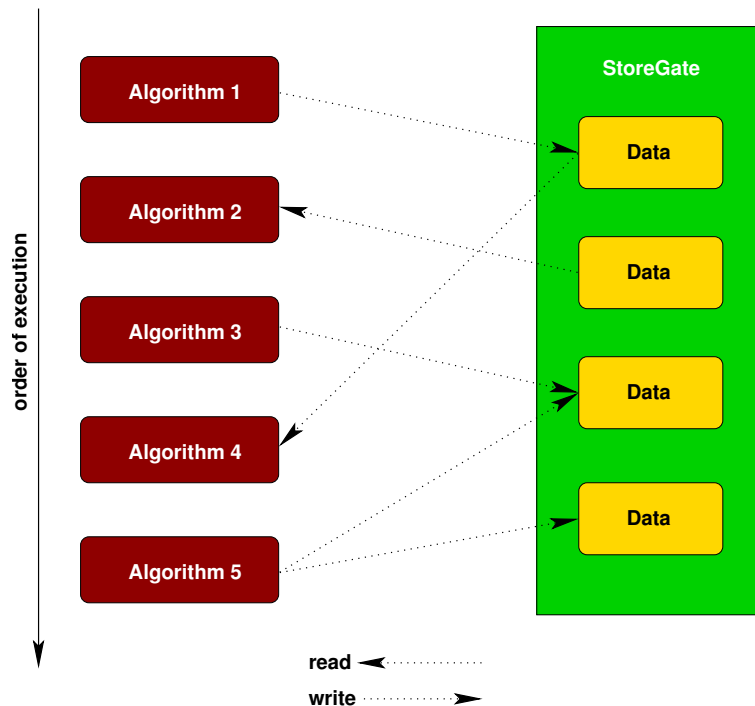


Figure 2.2: Data flow in Athena via StoreGate

Algorithms in particle physics tend not to be run separately, but to use many sub-algorithms for different data processing tasks. These sub-algorithms should run in an independent manner, rising the question of communication between algorithms. Athena uses the so-called *StoreGate* to make inter-algorithm communication possible (see figure 2.2). Algorithms are able to write and read from that dedicated store, but cannot modify any objects in StoreGate. This approach leaves memory management to StoreGate: Objects given to StoreGate do not need to be deleted explicitly (which is the cause of many memory leaks, as forgotten objects continue to consume memory), but are looked up on an event by event basis: If processing of one event is complete, StoreGate deletes the data connected with that. However, this is only true for event-processing algorithms. There are other Athena components which cannot be deleted after one single event, but have to remain accessible for the entire job. Therefore, there are other storage techniques in Athena, which work in the same way as StoreGate, but differ in their method of memory management.

The geometry description of the detector is such an example and storage management works here via *DetectorStore*. Describing the geometry data of the actual detector¹ correctly is crucial for each experiment, as it is the basis of both reconstruction and simulation. The ATLAS software framework contains the Geometry Model (*GeoModel*), where geometry data, as well as material properties, can be used to describe the actual detector. The *GeoModel* is designed as an ordered tree, where one can build up a hierarchical detector model (depicted in figure 2.3). The *World Volume* marks the top node of that tree. In the case of how the Munich

¹mainly ATLAS, but also ATLAS sub-experiments like the measurement facility in Munich

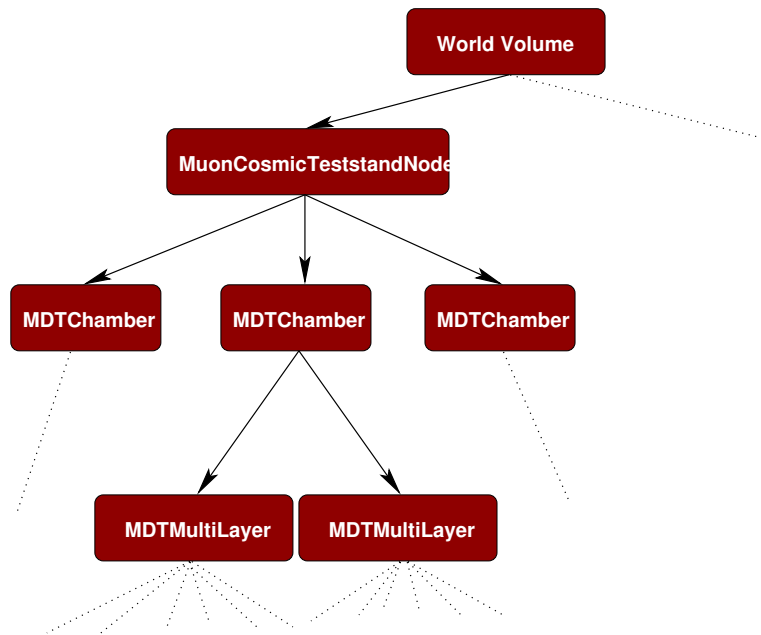


Figure 2.3: Tree structure of the Athena Geometry Model, as utilized in the MCT package

Cosmic Ray Measurement Facility is represented in the detector store, the next node is the `MuonCosmicTeststandNode`. Subsequent branches are `MDTChamber`, `MDTMultiLayer`. The different objects are addressed with a unique identifier tag. There also exist several types to classify sub-nodes by shape and material.

To handle differences between the real world and the nominal geometry description, Athena utilizes a conditions database `CondDB`. Different calibration data is obtained from detector elements and can then be applied in order to do correct reconstruction with Athena. Calibration data can be inserted into the Athena `CondDB`. The respective conditions database is specified in the joboptions and the corresponding calibration data are applied automatically. A related Athena feature is the Interval Of Validity Service. In high-energy-physics, a great deal of accuracy for the experiments has to be achieved, making fluctuations in environmental conditions, such as temperature, very critical. Small changes, usually in the micrometer range, have to be monitored and corrected. The Munich Cosmic Ray Measurement Facility is subject to another factor which causes disturbances in the alignment: Due to its purpose, the test chamber is exchanged weekly and the setup is repeatedly subjected to perturbations. Together with environmental fluctuations, a steady re-alignment is necessary. Therefore, event data have to be connected to the respective alignment and calibration data.

Athena solves this issue by introducing an Interval Of Validity Service, the `IOVsvc`. Once there is data registered in the `IOVsvc`, *from-* and *till-* run- and event-numbers are produced, which define the validity of corresponding conditions data. Once an interval expires, new conditions data has to be used. The updating of Interval of Validity data is performed automatically and prevents the user from using wrong conditions data in a transparent way.

2.2 MCT overview

By relying on the Athena framework, the MCT package makes extensive use of tools that already exist, thereby gaining valuable insight into ATLAS software concepts and their implementations.

2.2.1 Simulation in the MCT package

To gain accurate predictions for an experiment, a well-developed and sophisticated simulation of physics processes is required. Such simulation should produce signal data which accurately mimics the actual experiment, ideally making experiment and simulation indistinguishable. Data acquired by simulation can then be processed like detector data.

The trigger configuration at the Cosmic Ray Measurement Facility in Munich allows only one event at a time to be read. Thus, particle generation can be handled rather easy in the MCT package. The algorithm `SingleParticleGun`, a standard Athena particle generator, is used and produces random muon data.

To do particle tracking in simulation, some compatibility work is required with respect to the underlying Geant4 framework. Some special algorithms set the simulation boundaries and take care of compatibility with Geant4, where the relevant Geant4-Algorithms are to be used for simulation. Further procedures do the conversion to the Geant4 geometry description.

Simulating trigger behavior correctly is also of vital importance. The event-based hits stored are looked upon and scintillator digits and trigger signals are calculated with respect to event data.

The event that has been simulated has to be converted into digit information. Furthermore, the electronic setup is taken into account. In order to get accurate simulation data, additional corrections have to be applied to hit information data. These corrections consider signal run times along the tube wires, as well as signal run times in the electronics and cable setup. Having performed these calculations, the data set is smeared by a Gaussian distribution (as well as streamer and scintillator hit data) and converted into digits, given in units of TDC counts.

2.2.2 Track reconstruction using the MCT package

To do track analysis, data obtained from either simulation or the actual experiment, has to be processed in reconstruction algorithms. Raw simulation and experiment data are stored in digits and several steps are necessary in order to compute muon track information from this digit information.

- Initialization of the MCT detector description. The MCT package provides a Geometry Model that relies on the *GeoModel* concept used in Athena.
- Run-time corrections. The actual reconstruction process starts out from raw data, which is the information that is actually produced by the detector, given in TDC counts. This is information about time differences between the MDT drift tube signal and the scintillator signal. In general, this is a positive number, due to the effect of signal propagation time and signal formation. Signal propagation

times in chamber electronics are corrected for, as well as the signal propagation time along the tube wire. The latter correction is done by performing a rough track fit using scintillator information, in order to obtain information about the x coordinate of the muon trajectory. This track fit also provides information about the z coordinate of certain hits. Time-of-flight-corrections can then be applied, since the muons travel at finite speed ($\beta \geq 0.98$ for muons fulfilling the trigger requirement of 600 MeV). These corrections leave the bare *drift time*, which is the time the ionized, amplified electron cloud, originating from the muon passage, needs to reach the wire. Further corrections, obtained from additional calibration runs, have to be applied in order to determine drift time offsets.

- Translation of drift times into drift radii. By using a calibration file which relates drift times to drift radii (the so-called *r-t-relation*), that is, the distance of the origin of muon ionization to the MDT wire, each drift time can be converted into a drift radius. The r-t-relation depends highly on the actual MDT chamber properties, as well as on environmental conditions and has to be adjusted specifically.
- Pattern finding. Subsets of drift circles (which are the circles defined by drift radii) are assigned to possible muon trajectories in the pattern finding process. Local patterns, where sets of drift circles, whose centers show a distance from a given straight line less than a certain value, are stored as local hit patterns, whereas global patterns are stored by using overall subsets of all three chambers in the measurement setup. Further constraints are applied to the pattern finding process, such as possible hit patterns must consist of no less than 5 hits per chamber.
- Chamber alignment. By applying alignment parameters via the Conditions Database mechanism, which contains chamber-wide alignment information obtained by specific alignment runs (see chapter 3), the measurement setup is calibrated to fit the detector description. Shifts, originating from tolerances in chamber insertion are eliminated in the alignment process.
- Track fitting. Hit patterns are taken from the store and a track fit is performed. This is done for a global track fit through all chambers, as well as for local track fits, where separate trajectories are calculated for each chamber. The track fits are achieved by determining different parameters in a set of linear equations

$$\begin{aligned}x(z) &= m_x \cdot z + b_x \\y(z) &= m_y \cdot z + b_y\end{aligned}$$

Slopes m_x and m_y , as well as intercepts b_x and b_y (see figure 3.2) are determined. m_x and b_x are calculated by using a scintillator track fit, since the MDT chambers themselves are not sensitive in x direction. m_y and b_y can be calculated by the MCT track fitting algorithm. The algorithm is not hard-wired to any fixed fitting procedure, but acts as an interface where different methods can be used. The fitting strategy can be defined in joboptions. `NumRecLineFitter` performs a linear regression using track points and has been used throughout this thesis.

- Production of ROOT N-Tuples. Fit results are stored in a ROOT tree. Several branches contain various track information calculated for each event, such as the actual track parameters, χ^2 - sums and hit patterns for both global and local track fitting results. These N-Tuples can be used to do wire displacement analyses.

2.2.3 MCT calibration issues

Data taken from the measurement facility setup is affected by different biases when compared to idealized detector descriptions and reconstruction algorithms. These biases need to be calculated and corrected in order to do reconstruction and precision measurements.

The most basic correction concerns drift time offsets. In general, each single tube shows an offset in its drift time spectrum, which has to be corrected in order to obtain positive drift times. A drift time spectrum for a single drift tube shows a typical distribution, consisting of well-defined, steep rising and falling edges. The rising edge (T_0) gives information about the offset, which can then be corrected to zero, while the falling edge corresponds to a maximum drift time (T_{max} , see figure 2.4). Both T_0 and T_{max} are also used in the conversion of drift times into drift radii in order to fit the distribution of drift radii to the actual dimensions of the drift tube.

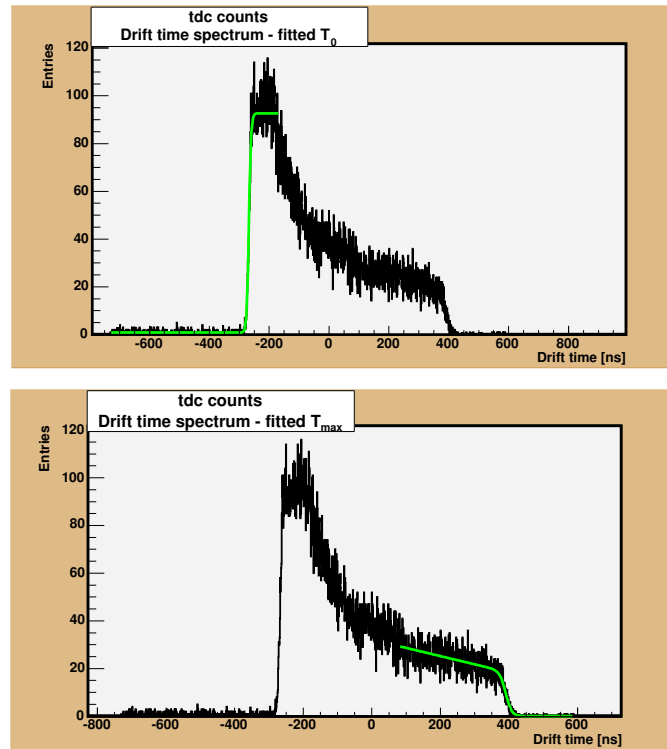


Figure 2.4: Drift time spectrum, including fitted Fermi functions to determine T_0 and T_{max}

To determine T_0 and T_{max} , the leading and trailing edges of the spectrum are parameterized by two Fermi functions:

$$G(\tau) = z_0 + \frac{A_0}{1 + e^{-\frac{\tau - T_0}{\tau_0}}}$$

$$H(\tau) = z_m + \frac{A_m - \alpha_m \tau}{1 + e^{\frac{\tau - T_{max}}{T_M}}}$$

where z_0 and z_m describe a flat background. τ_0 and T_M denote the slope at which the edges rise or fall while A_0 and A_m parameterize the height of the distribution. The linear function which describes the tail of the drift time spectrum is taken into account by $\alpha_m \tau$. The functions provide a means to calculate T_0 and T_{max} , which can then be taken and adjusted, such that the rise of the drift time spectrum occurs at zero drift time. Drift time corrections are inserted into the Conditions Database to be applied in subsequent reconstruction steps.

When computing drift radii from drift time data, the r-t-relation is needed. However, the r-t-relation is not universally valid for all chambers of a certain type, but has to be adjusted for each chamber and current environmental conditions. This is achieved by a standard, iterative process. Starting from a default r-t-relation, deviations between drift radii and track fits using this relation are considered. Systematic biases are corrected and new track fits are performed thereafter, thus finally leading to an r-t-relation that fits the actual chamber and measurement conditions. Figure 2.5 shows a significant slope in the distribution, while this slope has been eliminated by using a corrected r-t-relation (see figure 2.5).

Chamber alignment is another important calibration issue. Track reconstruction procedures rely on an idealized detector description, while data is taken from the real measurement facility setup. The real setup, however, is subject to shifts when chambers are mounted and other effects which cause significant deviations from the idealized setup. Therefore, specific alignment runs investigate systematic biases in reconstructed tracks in order to determine the parameters necessary to shift and rotate the chambers to their nominal positions. Those parameters are entered into the conditions database to be applied in reconstruction runs. This issue is discussed extensively in chapter 3

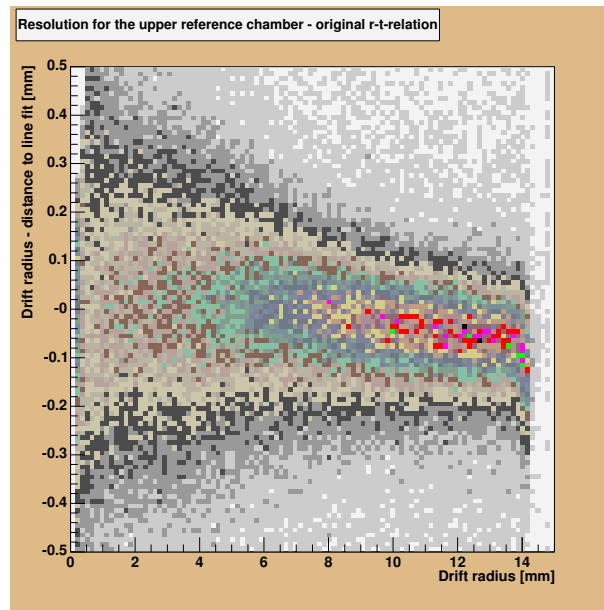


Figure 2.5: Difference of measured and fitted drift radii as a function of the measured drift radius.

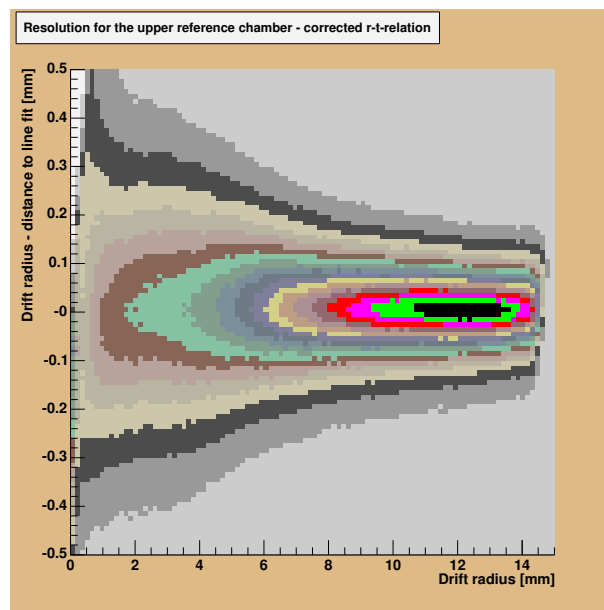


Figure 2.6: Difference of measured and fitted drift radii as a function of the measured drift radius, using a final r-t-relation.

Chapter 3

Chamber alignment and wire position analysis

In order to perform accurate track fits, alignment parameters of the MDT chambers in the measurement facility setup have to be taken into account. Five parameters for translation and rotation are determined by defining a reference frame, followed by aligning the MDT chambers with respect to that reference.

3.1 Alignment

3.1.1 Original chamber alignment

The MCT package is a functional software collection that allows track reconstruction using the ATLAS software framework. The principal functionality has already been described. Several steps are needed in order to progress from raw data to track information in a ROOT file. Within this process, calibration algorithms are of particular importance. The T_0 - corrections are the first calibration to be done, followed by additional r-t-relation adjustment and steps to address the chamber alignment. This process determines parameters that can be taken into account in order to treat differences between MDT chambers in the measurement facility setup and the MCT Geometry description.

A central assumption in the original chamber transformation algorithm is that the MDT chambers are regarded as rigid bodies, that is, no inner distortions in chamber geometry are considered. In the alignment processes, chambers are just aligned as a whole and there are no methods to take into account any intrinsic chamber deformations. Achieving a deeper level of alignment, such as looking at the multilayers to rule out any possibility of having a misalignment between them is not possible. Keeping this restriction in mind, the original MCT chamber alignment procedure contains the following steps:

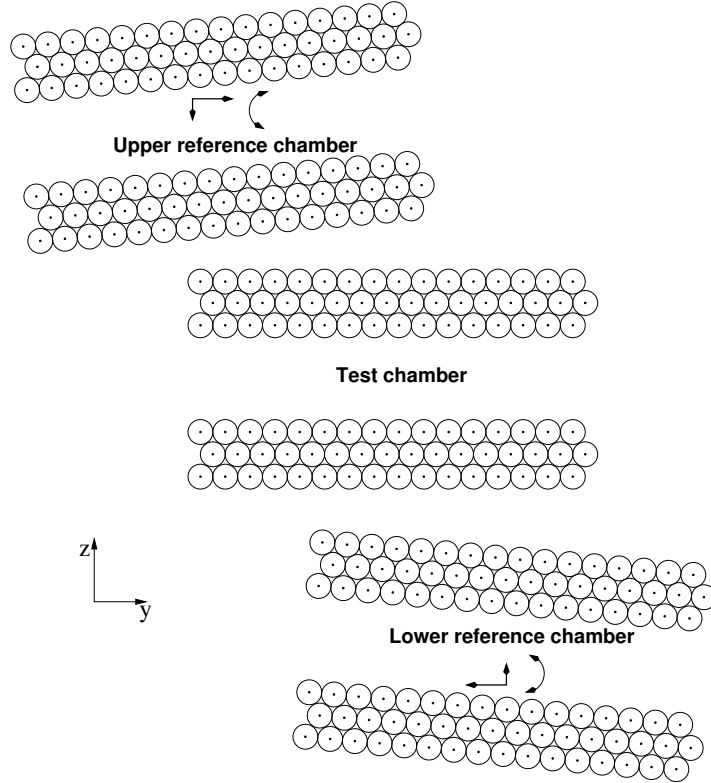


Figure 3.1: The existing Athena alignment procedure. The reference chambers are aligned with respect to the test chamber (Note: Not all 72 tubes per layer have been drawn here)

A reference frame is defined by the test chamber. The test chamber is taken as fixed and remains untransformed in the chamber alignment process. The upper and lower reference chambers are then transformed (see figure 3.1) with respect to the test chamber by a translation vector

$$T_{UC/LC} = \begin{pmatrix} 0 \\ \Delta y \\ \Delta z \end{pmatrix}$$

and a rotation matrix:

$$R_{UC/LC}(\alpha, \beta, \gamma) =$$

$$R^x(\alpha)R^y(\beta)R^z(\gamma) =$$

$$\begin{pmatrix} \cos \beta \cos \gamma & \cos \beta \sin \gamma & -\sin \beta \\ \sin \alpha \sin \beta \cos \gamma - \cos \alpha \sin \gamma & \sin \alpha \sin \beta \sin \gamma + \cos \alpha \cos \gamma & \sin \alpha \cos \beta \\ \cos \alpha \sin \beta \cos \gamma + \sin \alpha \sin \gamma & \cos \alpha \sin \beta \sin \gamma - \sin \alpha \cos \gamma & \cos \alpha \cos \beta \end{pmatrix}$$

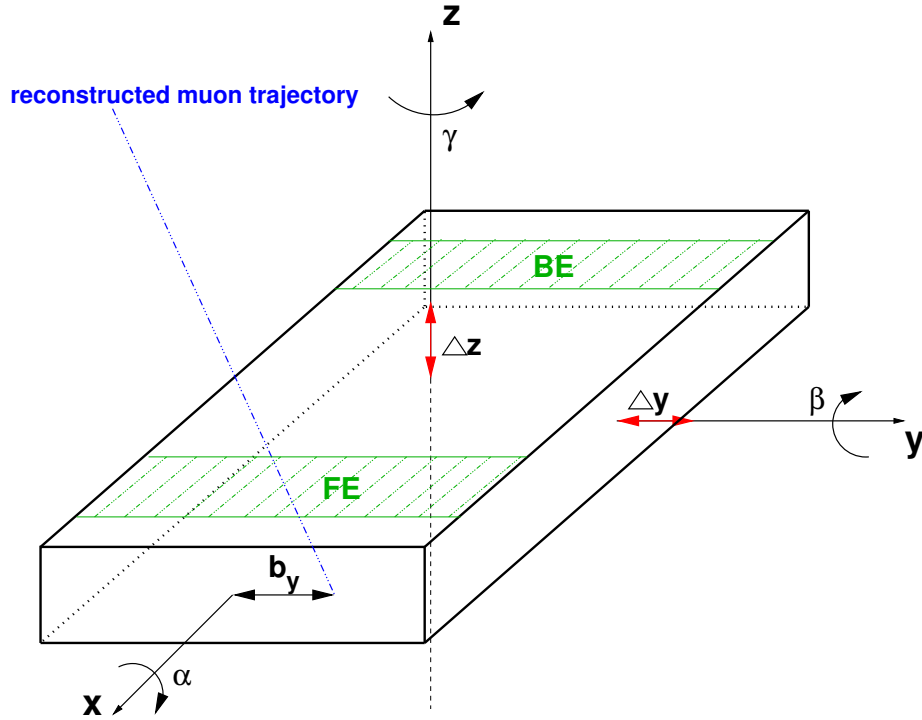


Figure 3.2: Definition of alignment parameters and other properties, as used in this thesis. The FE - and BE - areas denote front-end and back-end sections, defined in order to perform separate alignment calculations for each chamber end.

The first element of the translation vector is set to zero because the MDT chambers are not sensitive in the x -direction and therefore, no translation in this direction can be determined. See figure 3.2 for the definition of alignment parameters.

Translations along the y - and z -axis are calculated by considering differences between intercepts, that is, the parameter which gives information about the y impact coordinate of the track in the respective chamber. For the y - translation, the residuals of the intercepts b_y between test chamber (TC) and reference chamber (RC) are calculated event by event. These residuals are studied as a function of the slope m_y of the test chamber track.

$$\delta b = b_{y,TC} - b_{y,RC} = \Delta y + m_y \cdot \Delta z$$

An offset in this distribution corresponds to the alignment parameter Δy , while its slope translates into Δz (see figure 3.3).

Chamber rotations are determined in different ways: Firstly, the chamber rotation around the y - and z -axis are calculated by defining a *front end* (FE) and a *back end* (BE) section along the tube length (the x -position necessary for this purpose is determined by using scintillator information). The front end defines the tube area near the readout electronics, while the back end is the opposite, high-voltage side. The process described above is performed separately for both sections, resulting in y - and z -shifts $\Delta y_{FE/BE}$ and $\Delta z_{FE/BE}$.

The rotation angles around the y- and z-axis β and γ are then calculated by

$$\beta = \frac{\Delta z_{FE} - \Delta z_{BE}}{l_{Tube}}$$

$$\gamma = \frac{\Delta y_{FE} - \Delta y_{BE}}{l_{Tube}}$$

using a small angle approximation. Alignment rotation angles in the measurement facility are typically of the order 10^{-5} rad to 10^{-6} rad; thus, this approximation is justifiable and allows the angles to be calculated independently from each other.

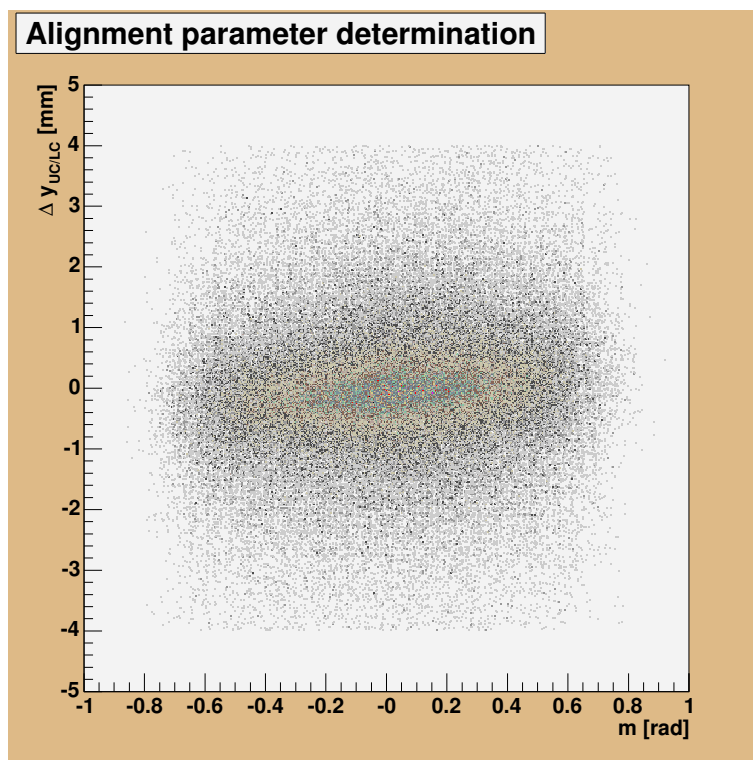


Figure 3.3: Delta intercept vs. slope distribution. Any slope along the x-axis has to be corrected for

The remaining parameter to be determined is the rotation angle around the x-axis. This angle is calculated from the differences of track slopes between test chamber and reference chamber. The mean value in this distribution corresponds to the x-axis alignment angle. The class `HepTransform3D`, taken from the CLHEP library [9], is used to store alignment parameters and performs the conversion into Euler angles.

In practice, problems arise when using this alignment process. This method has been introduced and tested in [14], where the alignment was performed in this way. There, wire position deviations obtained from these procedures were compared with tomograph data. In general, a good agreement between MCT analysis data and tomograph data was attained, but some effects remained to be understood.

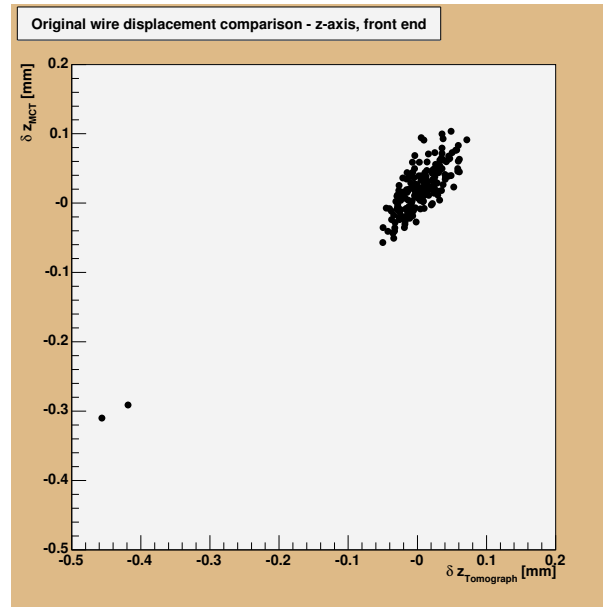


Figure 3.4: Comparison between MCT data and tomograph measurements in z direction. Note the 2 outliers on the bottom left of the distribution.

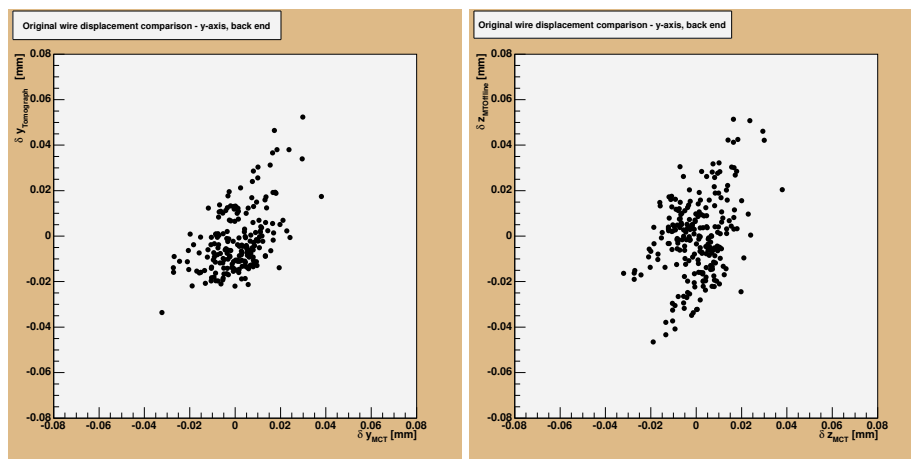


Figure 3.5: Comparison between MCT data and tomograph respective MTOOffline measurements. A double structure can be observed, in particular when comparing MCT and MTOOffline.

A comparison of front-side wire position deviations in z-direction between MCT and tomograph data shows two wires deviating significantly between both measurement methods: For these two tubes, the MCT analysis results in a wire displacement of about $300 \mu\text{m}$ compared to values of $400 - 500 \mu\text{m}$ obtained via tomograph measurements (see figure 3.4).

Another effect can be seen when comparing wire position deviations in the y-direction, particularly on the back side. In this case, comparison between MCT and tomograph data reveals some kind of "double structure". This creates a problem when trying to reach the required precision which needs to be understood (this double structure can be seen more clearly when comparing the MCT analysis with MTOOffline, see figure 3.5).

3.1.2 Introducing a new alignment procedure

Considering the existing alignment procedure in the MCT package, a major problem is found: Out of the three MDT chambers in the Cosmic Ray Measurement Facility, the middle chamber is taken as reference. But this chamber is actually the one which is changed frequently. Practical limitations when inserting the test chamber, as well as the occurrence of different errors in chamber geometry when changing the chamber, lead to the assumption that considering the test chamber as a rigid body to define the reference frame is unfavorable. There are many *possibilities* for internal MDT chamber deformations, which cannot be excluded a priori:

- When inserting the test chamber, small irregularities like dust particles between the suspension and the chamber can cause chamber torsions
- Mechanical tolerances during the chamber production are unavoidable
- Thermal effects, either caused by chamber electronics or by environmental conditions.

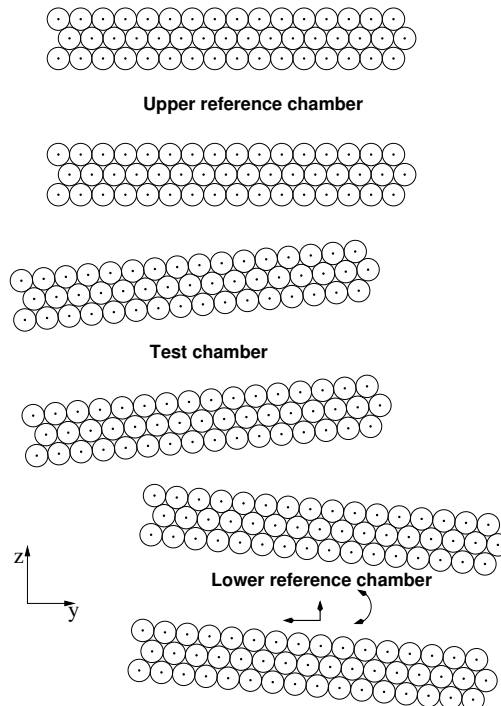


Figure 3.6: New chamber alignment. The test chamber is excluded from the alignment process

Using one of the reference chamber as the reference-origin should be better because they are, in contrast to the test chambers, not subjected to frequent modifications. In addition, tomograph data available for the reference chambers do not show significant deviations in chamber geometry.

Therefore, the alignment process in the MCT package underwent a major modification. The reference frame was changed to be defined by the upper reference chamber while completely omitting the test chamber in MCT alignment (see figure 3.6). The lower reference chamber is aligned with respect to the upper reference chamber whereas no track fits that are performed locally within the test chamber contribute to any alignment parameter.

This rules out the possibility of poor alignment results because of imperfections in the test chamber. However, since local track fits for the test chamber are no longer meaningful per se, additional work is required in the wire positions analysis in order to determine alignment parameters for the test chamber (see chapter 4).

3.1.3 Fit optimization in the alignment processes

Another issue to be addressed in the existing alignment process is the fact that, despite the alignment run itself is performed in an iterative way, one run is generally not sufficient to obtain sufficiently good results for the alignment parameters. Subsequent runs show that additional corrections are required, in particular when regarding the Δz alignment parameter. A rather large Δz correction (of several mm) is needed due to simplifications in the geometry description, and a misalignment of about $1 mm$ in Δz persists after one alignment run.

These shortcomings derive from a relatively broad scatter of the slope-delta-intercept relation, which is used to determine alignment parameters (see figure 3.7).

When performing an ordinary, linear least squares fit through this distribution, many outliers significantly affect the fit result, such that the slope of the 1st degree polynom fitted appears to be flatter than desired. Outliers are weighted in square, just as every other data point. Since asymmetric distributions emerge from technical limitations, such as quality cuts within the pattern recognition process, the fit result can be pulled towards lower slopes.

To reduce this effect, a method, proposed by Volker Blobel [11] was introduced. A variance cut is applied to clean up the data in order to get a proper set for the fit process. This happens as follows:

- Perform an ordinary fit through the data in order to get a first guideline for the cleaning process.
- Starting from this linear fit, a first cleaning step can be done: all outliers, i.e. the residuals r_i , which deviate by more than some factor c of the distribution's standard deviation σ , are either omitted or relocated on the border of the area "allowed":

$$y_i^* = \begin{cases} y_i & \text{if } |r_i| \leq c\sigma \\ \hat{y}_i - c\sigma \text{ or omitted} & \text{if } |r_i| < -c\sigma \\ \hat{y}_i + c\sigma \text{ or omitted} & \text{if } |r_i| > +c\sigma \end{cases}$$

y_i^* denotes "cleaned" data points, while y_i and \hat{y}_i stand for original data points and data points derived from the fit result respectively.

- With the resulting, new set of data, another fit can be performed
- Another variance cut is applied on the *original data* in the same way as before. Re-using original data to do the next variance cut is essential, otherwise, unexpected biases can occur when just using data cleaned up before.
- This process is iterated several times until the results get stable.

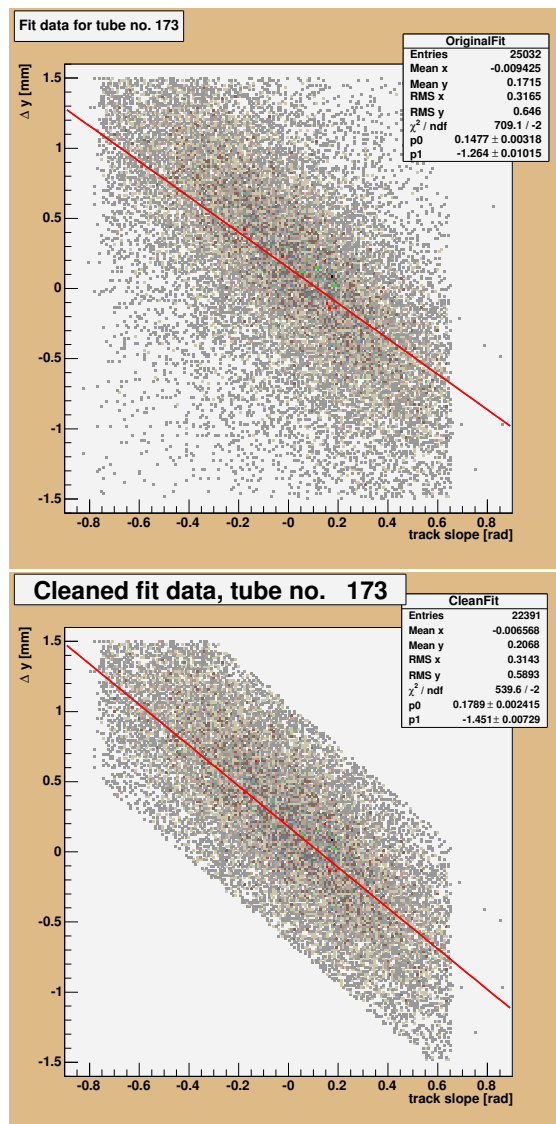


Figure 3.7: Comparison between performing an ordinary linear fit and doing so after cleaning up the data

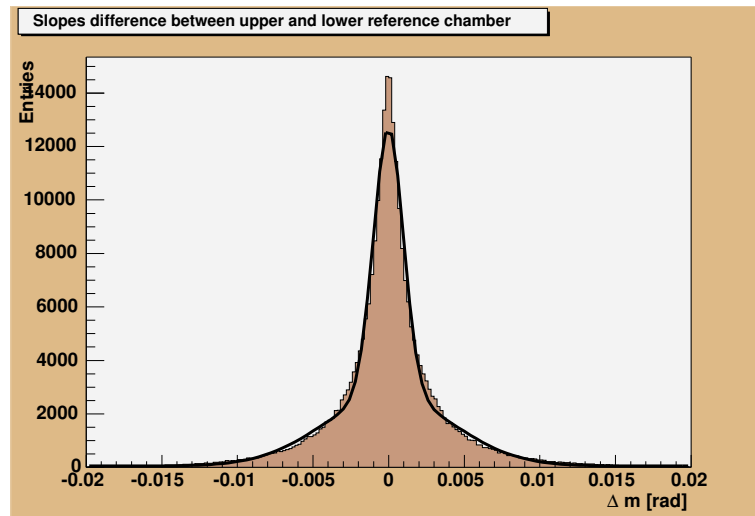


Figure 3.8: Composite function, fitted on the slope distribution to obtain a stable mean value

The procedure is illustrated in figure 3.7. For this application, good results are obtained for $c = 1.7$ after 5 iterations. This *robust-least-squares-fit* showed a significant gain in convergence for the alignment process. After one alignment run, Δz misalignment is reduced to about $50 \mu m$, in contrast to $1 mm$ in the original alignment algorithm.

Additional improvements have been made in order to gain accurate results when determining the x-axis rotation angle. The existing alignment process utilizes a standard, arithmetic mean. This method is rather sensitive to asymmetric outliers in the delta-slope distribution, which lead to biased mean values.

Therefore, a novel approach has been implemented in order to determine that alignment parameter. A composite function, consisting of two gauss distributions sharing a common mean and a linear background function

$$f(x) = b + x \cdot m + c_n \cdot e^{-\frac{(x-\mu)^2}{2\sigma_n^2}} + c_w \cdot e^{-\frac{(x-\mu)^2}{2\sigma_w^2}}$$

was used, c_n, c_w, σ_n and σ_w denoting constants and standard deviations of the "narrow" respective wide Gauss function, while μ denotes the common mean value. Fitting this function on the delta slope distribution (see figure 3.8) provides a more stable mean value which is then used as the x-axis rotational alignment parameter. As figure 3.8 shows, the function fitted does not reproduce the data perfectly. However, the purpose of the fit is to reduce background biases.

These procedures are undertaken in order to align the lower reference chamber with respect to the upper reference chamber. However, with the test chamber remaining in its original status, additional calculations are performed within the wire displacement analysis (see chapter 4).

3.2 Determination of wire displacements

3.2.1 Determination of wire position deviations in the test chamber

Once satisfactory alignment parameters have been determined, they can be registered in the Athena conditions data base. A full Athena run is done then, as described in chapter 2, in order to produce ROOT N-Tuples containing information about muon tracks that have been reconstructed. These tuples are used to do wire position analyses. For the event analysis of the data sample provided by the MCT package, some quality cuts have to be applied:

- slope differences, when comparing local track fits in the upper and lower reference chambers, must not be greater than 15 mrad
- differences in the intercepts of local tracks in the upper and lower reference chambers lead to the omission of the event when this difference is greater than 4 mm
- Local track fits of the upper and lower chamber are required to show a χ^2 - probability greater than 10^{-3} .
- Tubes at the borders of the MDT chamber show a lower angular acceptance. Therefore, muon tracks can be detected only in a relatively small slope range, which limits statistics, and finally the resolution, greatly. Therefore, data originating from one of the 16 tubes on each edge and on each layer are not used.

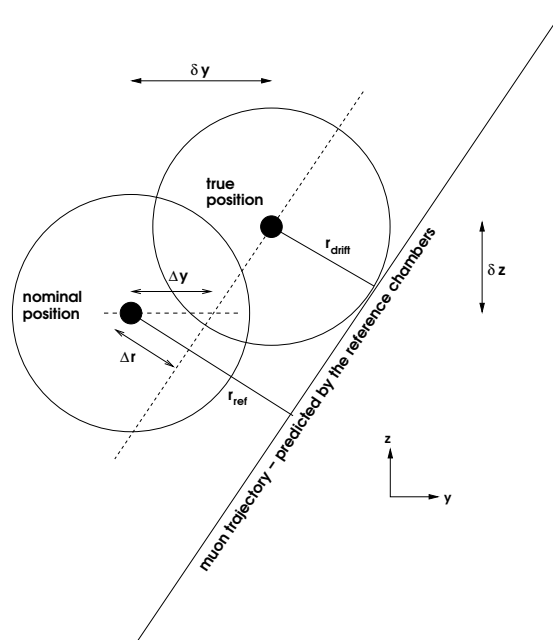


Figure 3.9: Drift radius predictions and their offset with respect to hit data obtained from the test chamber provide information about δy and δz , dependent on the slope of the muon trajectory. Figure taken from [14]

The wire position analysis now compares measured drift radii and drift radii predicted by the global reference chamber track fit. As depicted in figure 3.9, a dependence between the track slope m and the residuals of measured drift radii and predicted drift radii Δy can be derived:

$$\Delta y(m) = \delta y + \delta z \cdot m$$

An offset in the slope-delta-y-distribution corresponds to a wire displacement δy in y-direction, while the slope of the distribution provides the displacement δz of that wire in z-direction.

3.2.2 Test chamber alignment on analysis level

The original procedures for the wire displacement determination had to be expanded due to the changes in the alignment process. Having the test chamber completely unaligned by now means that the wire displacements δy and δz are no longer meaningful, as they contain several biases, originating from different alignment parameters. The fit procedures to determine wire displacements utilize the robust-least-squares-fit (see chapter 3.1.3) due to similar reasons as in the alignment process.

A major part of the new wire displacement analysis therefore concentrates on the determination of alignment parameters on different levels. Different calculations are performed:

- Re-building the overall alignment of the test chamber on analysis level. The whole chamber is regarded as a rigid body
- Determination of alignment parameters for further multilayer alignment, restricting the rigid-body-assumption to a multilayer level. Multilayer tilts and misalignments are calculated and corrected for
- Applying further corrections, now regarding single layers as rigid bodies, since tilts and misalignments can occur here, too.
- Investigate further alignment parameters which cannot be described by rigid bodies. A correction for "twists" between the chamber ends (in x-direction) is calculated and applied.
- Determination of tube-spacing effects. Alignment parameters concerning layers whose tubes are not arranged exactly parallel with respect to each other are determined.

Those issues are discussed in detail in chapter 4.

Chapter 4

Classification of MDT alignment parameters and their determination

It was found that a global rigid-body assumption (as described in chapter 3) is not sufficient for all chamber deformations which occur in practice. Some effects, originating from intrinsic deformations in the chamber geometry, require additional corrections. Therefore, the new wire positions analysis software follows the hierarchy of the MDT setup and introduces different levels of corrections, supplemented by corrections which do not allow the rigid-body assumption.

Aside from actual chamber deformations originating from slight tolerances in chamber production, the chamber is subjected to thermal effects which can influence the alignment parameters. The Cosmic Ray Measurement Facility is located in an air-conditioned hall to provide stable thermal conditions throughout the data-taking process. Measurements show that the temperature varies by no more than 1 K , even when regarding day/night temperature differences during summertime. Considering the thermal expansion coefficient given for aluminium in chapter 1.3.2, fluctuations in chamber geometry are restricted to the order of a few micrometers. Furthermore, thermal variations affect the test chamber as well as the reference chambers, therefore, the test stand setup is largely insensitive to these deviations.

A first-order correction takes effects into account which could arise from differences in thermal expansion coefficients in the whole test stand setup (including the support structure into which the chambers are inserted). The data sample used throughout this thesis is split up into several smaller sub-samples. Separate alignment parameters were calculated in order to obtain parameters that are better tuned to the respective environmental conditions.

Another source of temperature variations is the chamber electronics. The wires are connected to high voltage on one end and to readout electronics on the other end. The readout electronics produce some non-negligible waste heat which is greater than waste heat produced on the high-voltage side. This leads to "artificial" tube-spacing effects, since there is more thermal expansion on the read-out end than there is on the high-voltage side. However, these thermal expansions affects every chamber in a similar way, such that this particular tube-spacing effect gets largely canceled for

alignment studies based on reconstructed muon tracks.

4.1 MDT elements to be treated as rigid bodies

4.1.1 Global alignment on analysis level

The first process to be undertaken is re-modeling the original test chamber alignment procedure. Chamber alignment is based on a first rigid-body-assumption: The chamber as a whole can be translated and rotated, but all elements inside the chamber are assumed to be at nominal position with respect to the chamber. Thus, the average wire position deviations, taking all wires of the test chamber into account (excluding those omitted by angular acceptance cuts), correspond to a misalignment of the chamber. A non-zero mean value of global wire position deviations in the y-direction represents a translational misalignment Δy in that direction; the alignment parameter Δz can be calculated analogous.

Rotational parameters are determined by using mean values that have been calculated for sets of wire displacements on the front-end ($\Delta y/z_{FE}$) and back-end ($\Delta y/z_{BE}$) area:

$$\beta = \frac{\Delta z_{FE} - \Delta z_{BE}}{l_{eff}}$$

$$\gamma = \frac{\Delta y_{FE} - \Delta y_{BE}}{l_{eff}}$$

where l_{eff} denotes the effective tube length, that is, the difference of mean intercept parameters $\bar{b}_{FE} - \bar{b}_{BE}$. These mean intercept parameters are calculated by averaging the x-impact information for each event that contributes to either front-end or back-end fits.

A special procedure is performed in order to determine the x-axis rotation angle. In the MCT chamber alignment, this can be accomplished by using slope residuals. However, test chamber track parameters are not available for the wire positions analysis (because of the test chamber remaining un-aligned in MCT), so additional calculations are required. Wire displacements in the z-direction (δz) are studied along the y-direction. The slope of the distribution corresponds to the x-axis rotation angle α .

4.1.2 Multilayer misalignment and tilts

Having aligned the chamber on a global scale, the next step is to consider wire displacement mean values that are calculated separately for each multilayer, divided into front-and back end wire displacements again. Front- and back-end multilayer corrections derived from the corresponding mean values are used to obtain the same set of parameters as determined on global scale, on multilayer level. These are $\Delta y_{ML1/2}$, $\Delta z_{ML1/2}$, $\alpha_{ML1/2}$, $\beta_{ML1/2}$ and $\gamma_{ML1/2}$.

Different geometry distortions can be identified by interpreting these parameters, if significant (i.e. showing a significant value when compared to their errors). The relationships

$$\Delta y_{ML1} = -\Delta y_{ML2}$$

$$\Delta z_{ML1} = -\Delta z_{ML2}$$

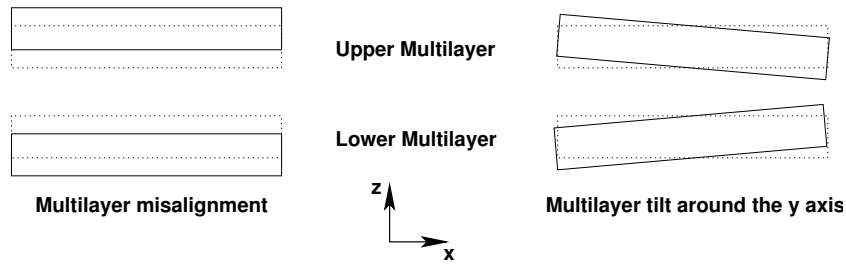


Figure 4.1: Schematic view of multilayers being tilted around the y-axis

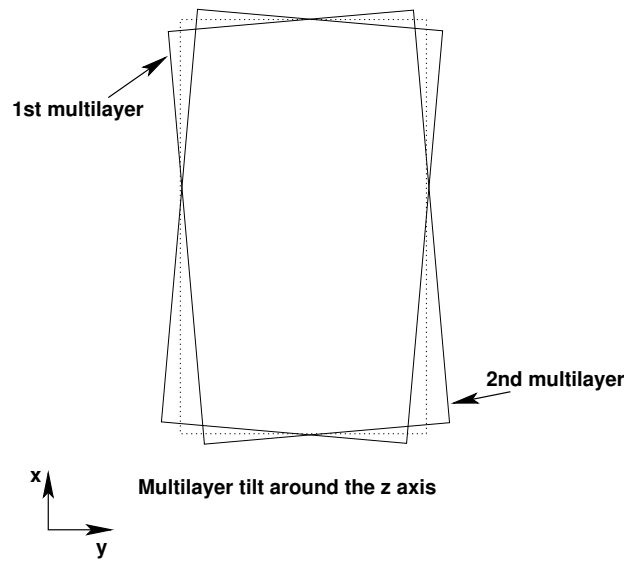


Figure 4.2: Schematic view of multilayers being tilted around the z-axis

translate into translational multilayer misalignments. Deviations in y-direction correspond to an offset between both multilayers, while multilayer displacements in z-direction show that the multilayers are either too close or too far away from each other.

$$\alpha_{ML1} = -\alpha_{ML2}$$

corresponds to a multilayer tilt, where the multilayers are not arranged parallelly with respect to each other. An analogous case is

$$\beta_{ML1} = -\beta_{ML2}$$

Figure 4.1 shows examples of possible geometry distortions. Multilayer tilts around the z-axis can be seen when

$$\gamma_{ML1} = -\gamma_{ML2}$$

now perceiving non-parallel wires between both multilayers (see figure 4.2)

4.1.3 Single-layer misalignment and tilts

The final step of decomposing the MDT chamber geometry into different levels is the determination of the alignment parameters on a single-layer level. Having done the global alignment, followed by correcting multilayer geometry distortions, each single layer is now considered as a rigid body. This establishes an additional category of alignment parameters to be calculated.

The distortions discussed for the multilayer level case may also be considered for the single-layer level, as different arrangements of one (assumed) cuboid with respect to another are studied here, too.

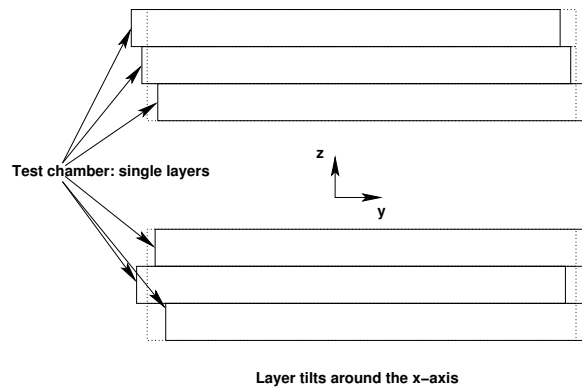


Figure 4.3: Outline of single layers showing offsets in y-direction

Since single layers are glued to each other, systematic misalignments between them are expected to be very small; nevertheless, it is useful to check. A single-layer tilt in the z- or y-direction is analogous to the multilayer case. Single layer misalignments, where one layer is shifted in y - or in z - direction when compared to the geometry description, are also possible. A further example of layer misalignment is shown in figure 4.3.

4.2 Non-rigid-body chamber deformations

The possibilities of differences between the nominal geometry description and the actual, assembled MDT chamber, are not confined to those which can be described by applying a rigid-body assumption. There are many possibilities which do not allow description by taking certain elements of the chamber as a whole. Two non-rigid-body cases have been observed.

4.2.1 Twisted chamber ends

An error in chamber geometry, where any considerations about rigid bodies fail, is the case where the chamber ends (i.e. the ends of the chamber the x-direction) that are assumed to sit solidly on the test stand's suspension, are twisted with respect to each other due to the fact that the suspension structure itself deviates from an idealized case.

Differences to the nominal geometry description are unavoidable, since the material the chambers consist of (aluminium) has a finite strength and a non-zero weight. So, the behavior of a MDT chamber does not behave like a wooden, four-legged table that stands on uneven ground. The table maintains its shape and can wiggle around, while the weight of the MDT chamber causes it to be distorted when inserted in a suspension that is not perfectly planar, introducing a torsion along the x axis. ¹

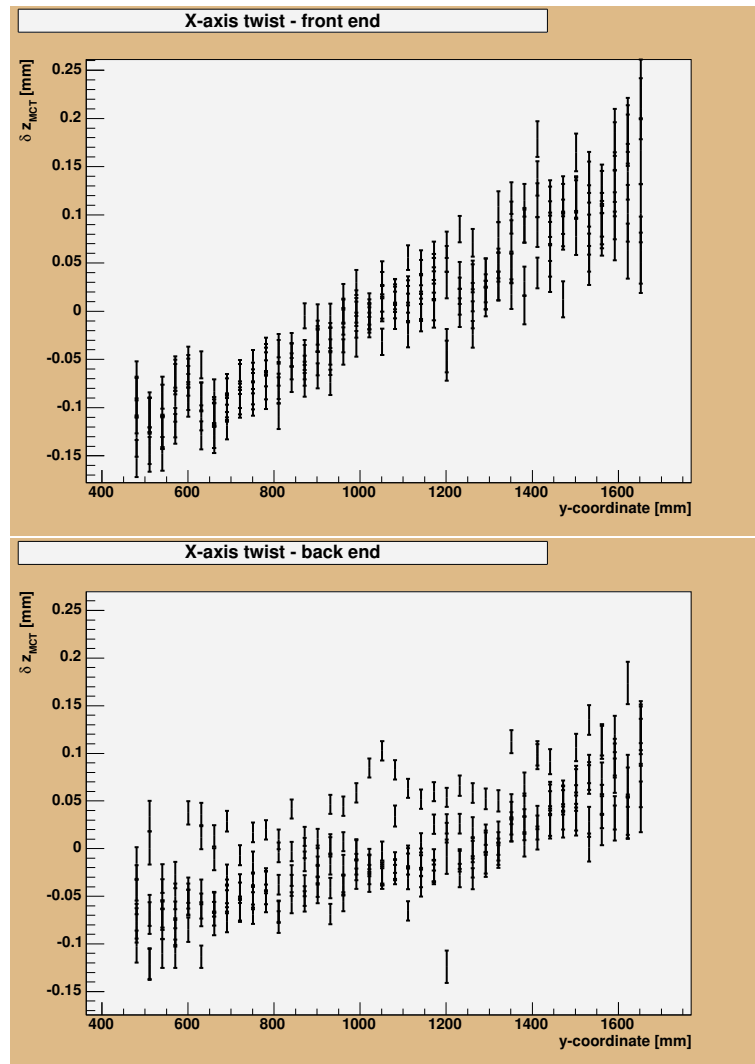


Figure 4.4: Impact of twisted chamber ends. z- wire displacements are shown as a distribution over the chamber width. Up to six values are associated with a specific y-coordinate due to the MDT chamber setup.

Special care is taken when inserting MDT chambers into the Cosmic Ray Measurement Facility, but even dust particles present between the suspension and the test chamber

¹actually, the analogy is not a perfect one, since the wooden table can be distorted just as well by several hundred μm

can cause deviations up to several hundred micrometers. This distortion is dependent on the respective setup and rather hard to reproduce.

This type of chamber distortion is addressed in the new wire positions analysis software. In a manner similar to the determination of the x-axis alignment angle (see chapter 4.1.1), z-wire position deviations are studied with respect to their y-coordinates. Two separate slopes for this distribution are determined, one on the front end and one on the back end (see figure 4.4). These slopes are used as additional alignment parameters and are corrected separately for each chamber end. Having already done the global x-axis alignment, these two slopes average to zero *per construction*; however, a twist around the x-axis is accounted for.

This correction proved to be the most valuable one in terms of understanding the problems that existed in the original alignment and wire position analysis procedures, as the x-axis torsion is responsible for producing double structures in the back-y section (see chapter 3.1.1). Using this new approach eliminates this effect.

4.2.2 Tube-spacing

Manufacturing the MDT chambers means maintaining a high standard of precision when producing the layers of 72 tubes each. However, small irregularities of the order of micrometers can add up systematically over the whole chamber width, displacing the 72nd tube wire by several ten micrometers with respect to the first tube. These irregularities do not necessarily occur in the same way on both chamber ends, such that tubes can be "fanned out" along the x-direction, as outlined in figure 4.5.

The correction for this possible chamber distortion is performed by studying the y wire position displacements as a function of the y-coordinate. The slope m_{TS} of the distribution parameterizes this effect:

$$\delta y_{i,TS} = m_{TS} \cdot y_{i,nom}$$

where $\delta y_{i,TS}$ denotes the correction applied to the i-th wire in a single layer and $y_{i,nom}$ is the nominal position of the i-th wire in y-direction. This correction is calculated and applied for wire displacements measured in the front-end and back-end area and for each single layer.

Such a tube-spacing effect is, at least in principle, also possible in the z direction. However, because there are only 3 layers of tubes, compared to 72 tubes in the y direction, the effect is expected to be much smaller. However, the presence of a gluing layer in the z-direction is an additional factor of uncertainty. Nevertheless, most tube-spacing effects in z direction should already be included in the single-layer corrections for z-wire position deviations applied before.

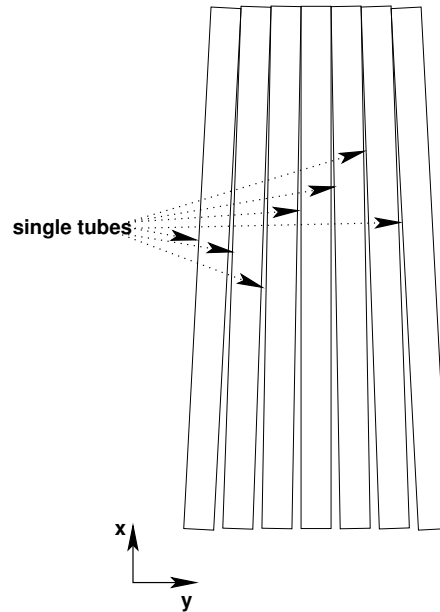


Figure 4.5: Schematic depiction of tubespacing effects

4.2.3 Remaining wire displacements

All systematic displacements related to effects at the MDT chamber-, multilayer- or layer-level are accounted for by the alignment parameters discussed so far. Any remaining displacements are due to individual tube wires.

Chapter 5

Results

The sample of raw measurement facility data used to develop the methods and processes discussed in this thesis, is comprised of 6.9 million events recorded using the BOS-4C-16 test chamber. The data was taken by the Munich Cosmic Ray Measurement Facility in January 2003, over a period of approximately 32 *h*.

The chamber was also scanned by the CERN X-Ray tomograph. Wire positions were measured at two points, each at a distance of 30 *cm* to the end of the chamber, with a precision of 2 μm .

5.1 Comparison: MCT alignment and wire position analysis to tomograph data

The data taken from the chamber BOS-4C-16 was chosen to be used due to the availability of tomograph data. Tomograph measurements are performed by taking the chamber as a whole into account, delivering "raw" wire displacement data. Therefore, the procedures to correct intrinsic alignment parameters were turned off to be able to reproduce tomograph data. The alignment is undertaken on a chamber-wide scale in the wire positions analysis. The paradigm of regarding the chamber as a whole to be consistent with tomograph measurements has been relaxed to allow corrections of twisted chamber ends. As stated in section 4.2.1, this deformation depends on local chamber placement and is probably not reproducible, thus making such a correction appropriate.

The front-end z-displacement distribution (figure 5.2) still shows 2 outliers which deviate from the diagonal, though the difference between the MCT analyses and tomograph measurements for these tubes is less pronounced than the difference observed when using the original alignment process. However, the deviations remain.

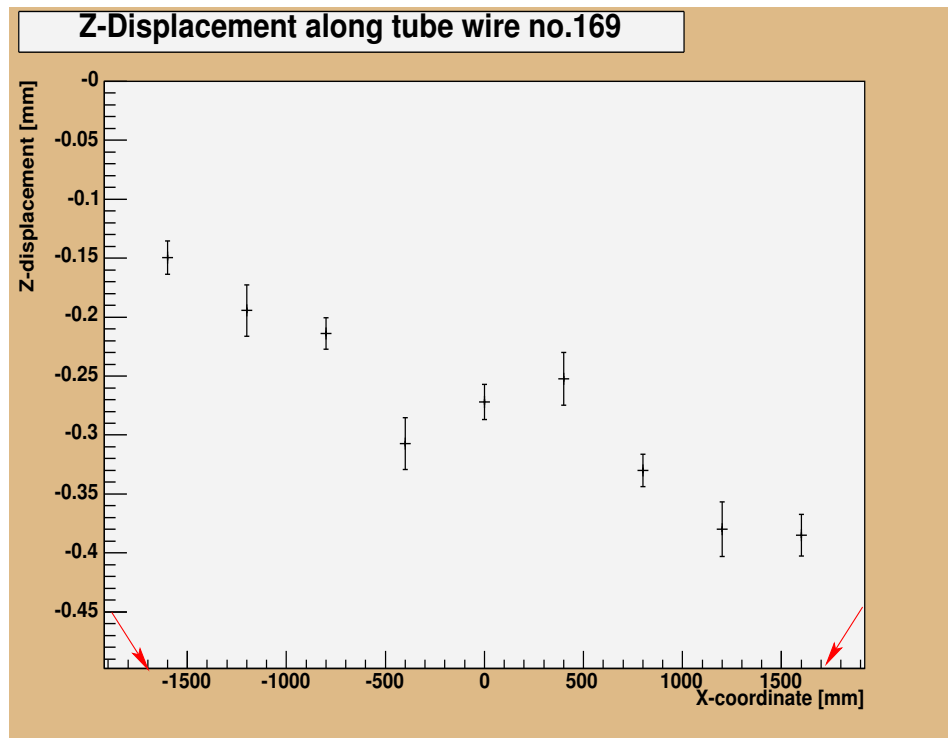


Figure 5.1: Front z displacements of a single tube wire, obtained by fitting several areas along the wire. The arrows denote the tomograph location of measurement

Figure 5.1 shows that these 2 tubes are special cases where the tube wire is strained at a relatively high angle with respect to the layer plane. This leads to problems in comparing MCT analysis and tomograph data: While wire displacements are measured at a set point 30 cm away from the tube ends in the X-ray tomograph, the MCT wire displacement analysis uses event information taken from a range of 1 m on each chamber end¹. Thus, the result of the determination of wire displacement is under-estimated in these special cases, when compared to tomograph data. Figure 5.1 was obtained by performing wire displacement calculations using wire sections of 20 cm along the whole wire. Linear extrapolation shows agreement with tomograph data at its actual location of measurement.

¹the section from 25 cm–125 cm in x-direction is the front-end area, while the section from 275 cm–375 cm represents the back-end area, with the origin of the x-coordinate being located at the tube end

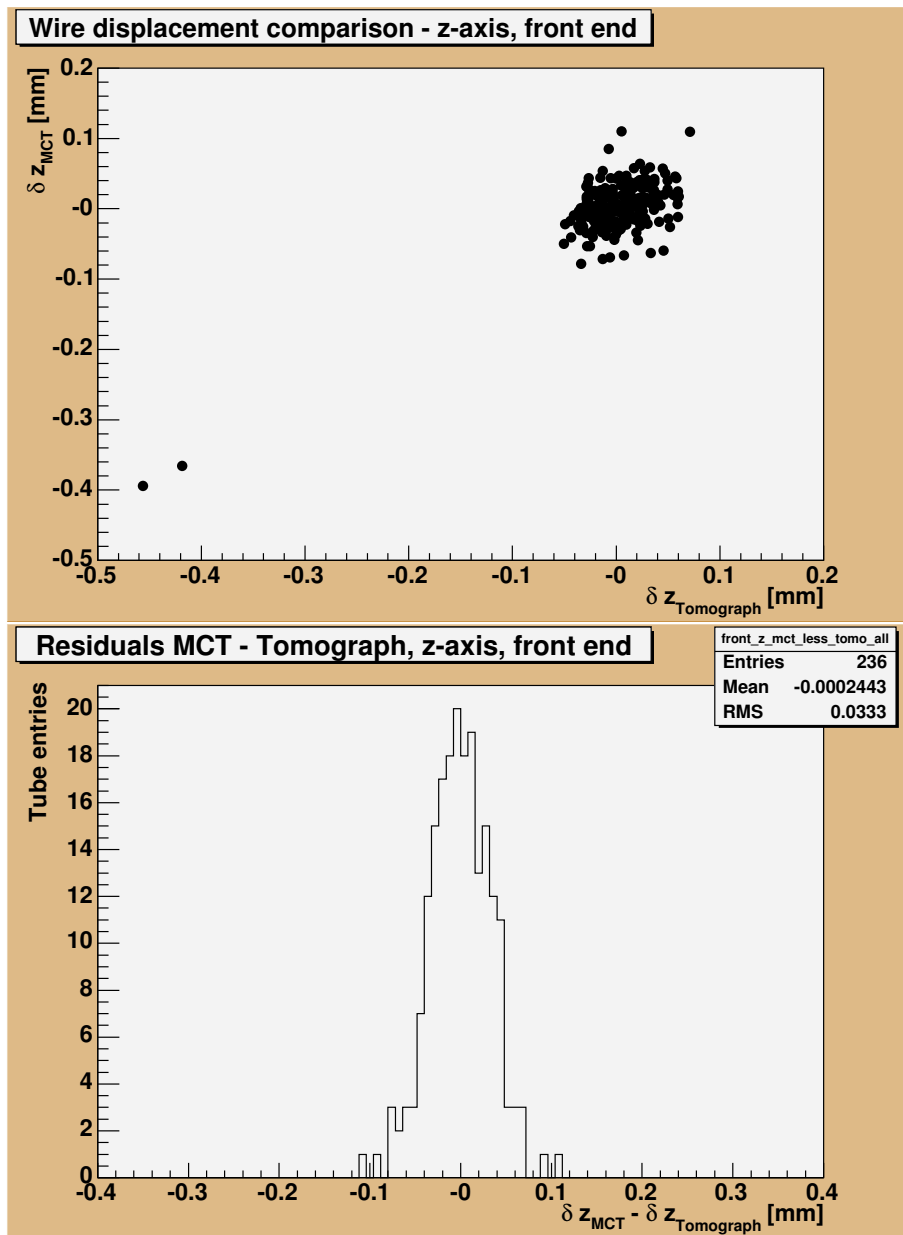


Figure 5.2: Comparison of MCT and tomograph front-z-displacement measurements and residuals.

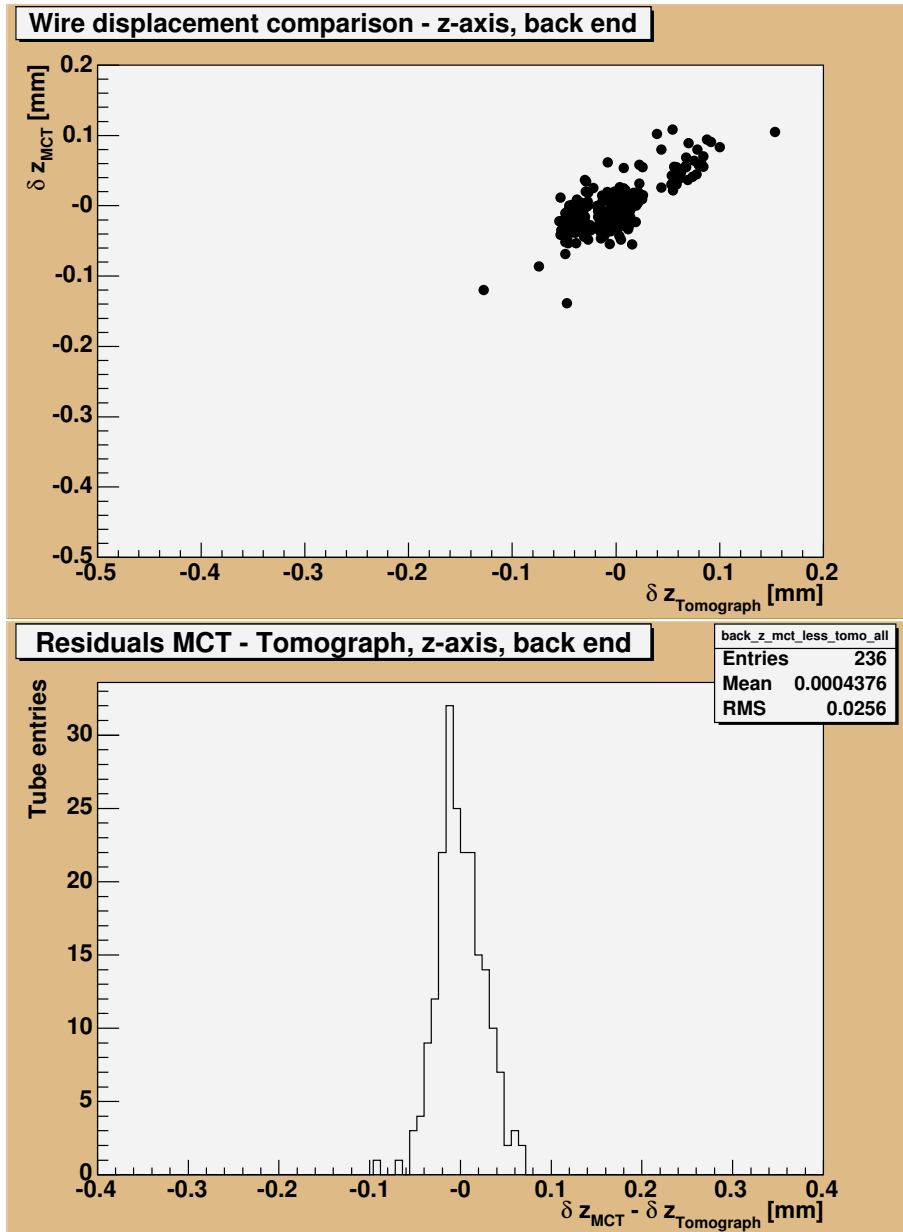


Figure 5.3: Comparison of MCT and tomograph back-z-displacement measurements and residuals.

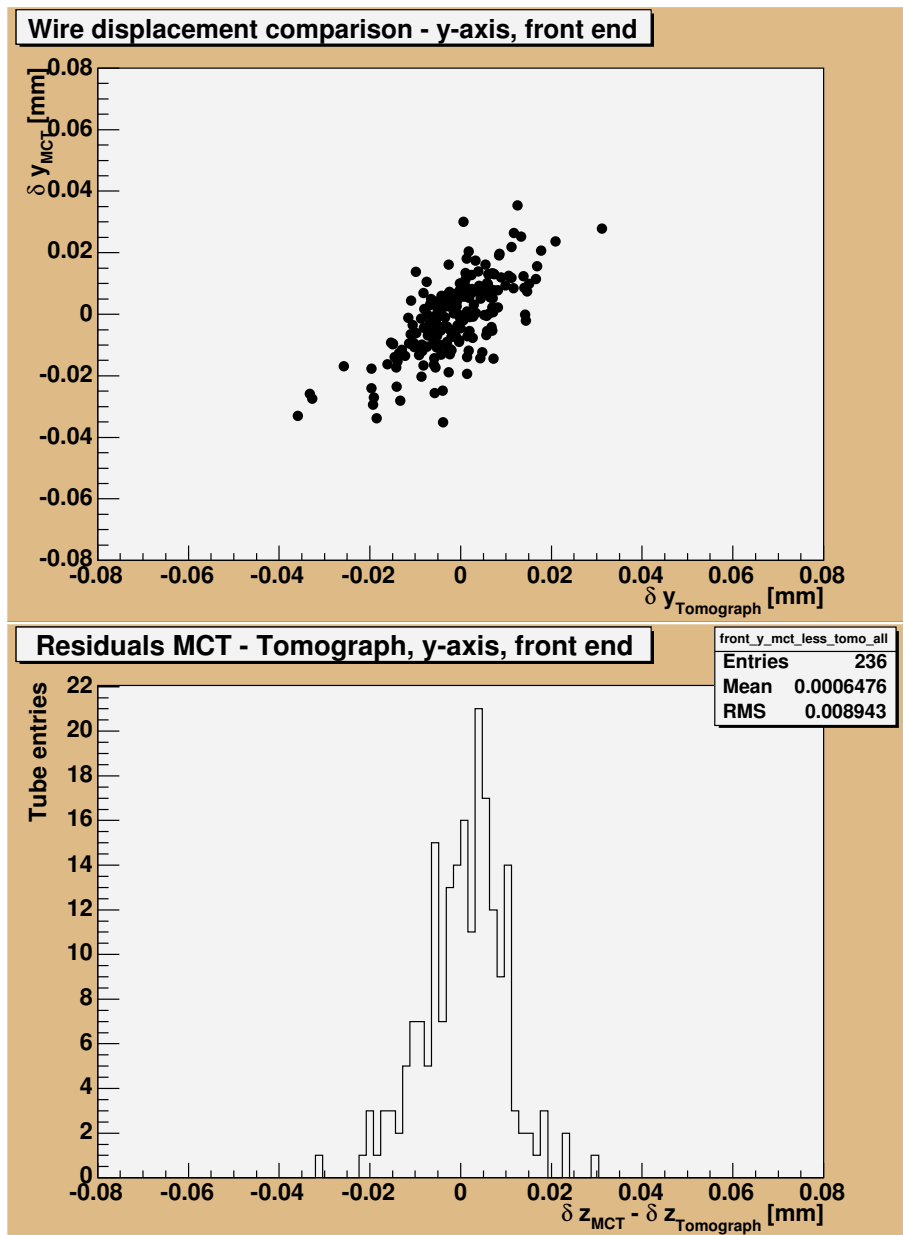


Figure 5.4: Comparison of MCT and tomograph front-y-displacement measurements and residuals.

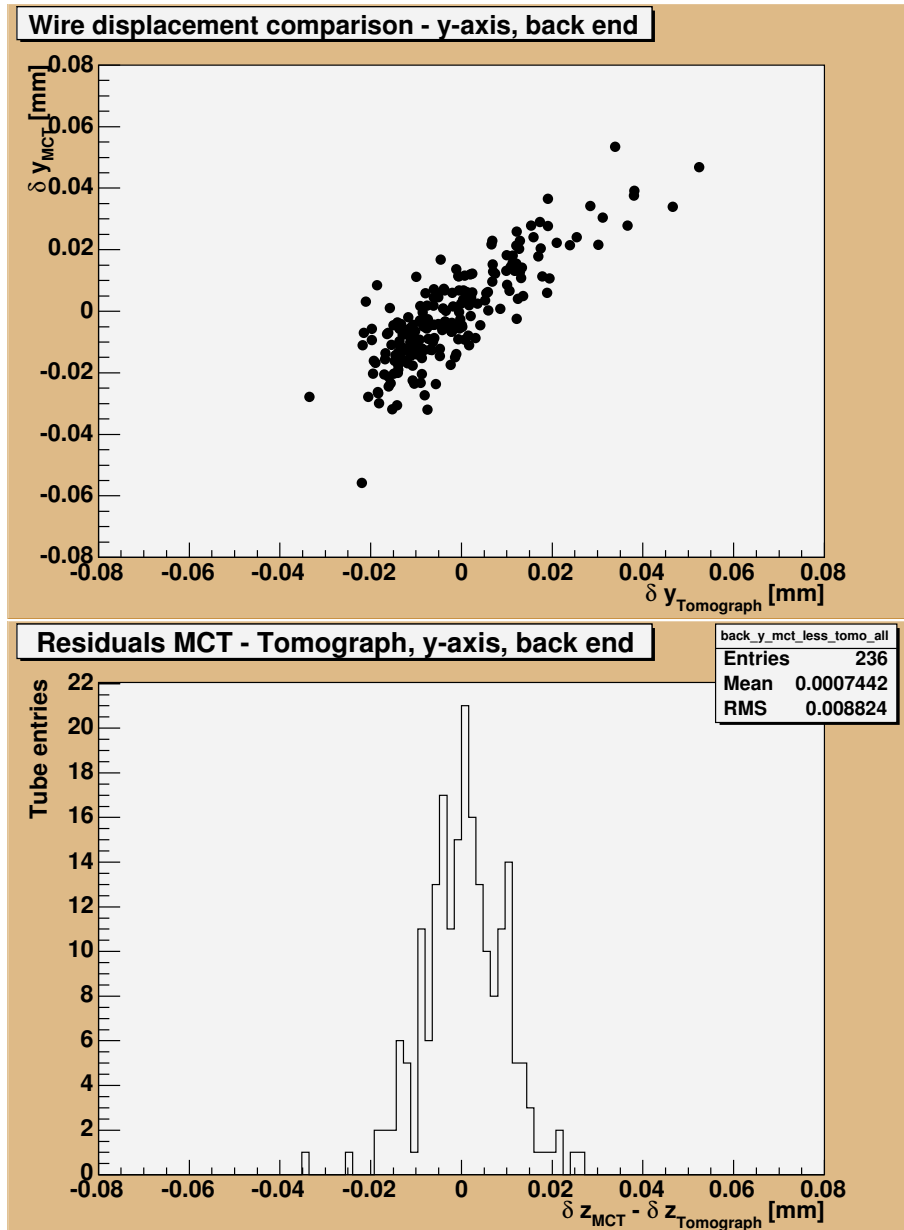


Figure 5.5: Comparison of MCT and tomograph back-y-displacement measurements and residuals.

Aside from the issue discussed above, the new procedures that have been implemented produce information about wire displacements that are in accordance with tomograph measurements. Both MCT and tomograph data are well correlated and resolutions of $9 \mu\text{m}$ and $30 \mu\text{m}$ for y- and z- displacement determination have been achieved in the MCT analysis procedures. Several subtle effects have been understood and eliminated, accompanied by the availability of means to determine systematic distortions in chamber geometry.

5.2 Numerical values for different systematic chamber geometry errors and discussion of the necessity for the calibration

The following tables contain the full set of alignment parameters calculated in the wire positions analysis. Parameters ΔY , ΔZ , α , β and γ are given for each level of alignment. Indexes $(M)Ln$ denote alignment parameters calculated on (multi-)layer-level, with n specifying the multilayer- or layer-number. Tubespacing parameters are given as slopes $m_{TS,Ln,FE/BE}$, obtained from studying y -displacements over the chamber width, in units of tube diameters. Translational alignment parameters are given in units of μm and rotation angles are given in μrad .

Global alignment parameters, chamber BOS-4C-16	
ΔY	147.20 \pm 0.20
ΔZ	1105.84 \pm 0.68
α	171.42 \pm 2.12
β	45.25 \pm 0.54
γ	44.98 \pm 0.16

Table 5.1: Alignment parameters calculated for a global rigid-body assumption.

Multilayer alignment parameters, chamber BOS-4C-16	
ΔY_{ML1}	4.96 \pm 0.26
ΔZ_{ML1}	14.16 \pm 0.92
α_{ML1}	16.89 \pm 2.97
β_{ML1}	-0.57 \pm 0.74
γ_{ML1}	4.64 \pm 0.21
ΔY_{ML2}	-4.92 \pm 0.27
ΔZ_{ML2}	-12.09 \pm 0.94
α_{ML2}	-17.41 \pm 3.02
β_{ML2}	1.97 \pm 0.75
γ_{ML2}	-4.74 \pm 0.22

Table 5.2: Alignment parameters calculated on a multilayer level.

In addition to the global alignment parameters, multilayer tilts show numerical values of up to several ten micrometers. A correction for significant distortions in chamber geometry may be appropriate. Having done those corrections, the remaining single-layer tilts are mainly in the region of few micrometers. Furthermore, statistical fluctuations

have a greater impact due to the increased effect of individual outliers. However, outliers in single-layer tilts are nevertheless existent due to a limited accuracy in the gluing process (see chapter 1.3.1). Thus, calibration on single-layer-level is not completely negligible.

Tubespacing parameters, when translated into displacement information, show values that again correspond to effects of single micrometers, even when regarded over the whole chamber width. This effect appears to be insignificant, since the values are comparable in size to their respective errors.

Layer alignment parameters, chamber BOS-4C-16		
ΔY_{L1}	1.96	± 0.49
ΔZ_{L1}	23.90	± 1.68
α_{L1}	-12.64	± 5.09
β_{L1}	-13.76	± 1.34
γ_{L1}	-3.50	± 0.39
ΔY_{L2}	-8.58	± 0.49
ΔZ_{L2}	-7.65	± 1.68
α_{L2}	-4.21	± 5.11
β_{L2}	0.035	± 1.34
γ_{L2}	4.39	± 0.39
ΔY_{L3}	-3.95	± 0.49
ΔZ_{L3}	-24.72	± 1.71
α_{L3}	23.85	± 5.23
β_{L3}	9.90	± 1.37
γ_{L3}	-1.07	± 0.39
ΔY_{L4}	-0.72	± 0.51
ΔZ_{L4}	6.91	± 1.74
α_{L4}	-6.33	± 5.48
β_{L4}	0.053	± 1.39
γ_{L4}	0.70	± 0.40
ΔY_{L5}	-3.17	± 0.51
ΔZ_{L5}	-1.15	± 1.73
α_{L5}	5.78	± 5.15
β_{L5}	1.13	± 1.38
γ_{L5}	-1.3	± 0.41
ΔY_{L6}	-7.71	± 0.51
ΔZ_{L6}	-8.65	± 1.72
α_{L6}	2.34	± 5.13
β_{L6}	-0.87	± 1.38
γ_{L6}	0.91	± 0.40

Table 5.3: Alignment parameters calculated on a single-layer level.

Special alignment parameters, chamber BOS-4C-16		
α_{FE}	229.79 ± 3.30	Twisted chamber ends
α_{BE}	113.04 ± 2.65	
$m_{TS,L1,FE}$	$(-389.96 \pm 68.09) \cdot 10^{-6}$	Tubespacing
$m_{TS,L1,BE}$	$(-320.73 \pm 51.71) \cdot 10^{-6}$	
$m_{TS,L2,FE}$	$(-199.69 \pm 68.20) \cdot 10^{-6}$	
$m_{TS,L2,BE}$	$(-48.74 \pm 51.90) \cdot 10^{-6}$	
$m_{TS,L3,FE}$	$(-18.01 \pm 69.52) \cdot 10^{-6}$	
$m_{TS,L3,BE}$	$(378.56 \pm 53.11) \cdot 10^{-6}$	
$m_{TS,L4,FE}$	$(-223.63 \pm 73.50) \cdot 10^{-6}$	
$m_{TS,L4,BE}$	$(202.75 \pm 56.90) \cdot 10^{-6}$	
$m_{TS,L5,FE}$	$(5.16 \pm 70.12) \cdot 10^{-6}$	
$m_{TS,L5,BE}$	$(-71.11 \pm 54.52) \cdot 10^{-6}$	
$m_{TS,L6,FE}$	$(-578.79 \pm 69.86) \cdot 10^{-6}$	
$m_{TS,L6,BE}$	$(-103.55 \pm 54.13) \cdot 10^{-6}$	

Table 5.4: Alignment parameters concerning twisted chamber ends and tubespacing effects.

Chapter 6

Summary

The Munich Cosmic Ray Measurement Facility was installed in order to calibrate ATLAS monitored drift tube (MDT) chambers for deviations in their wire positions and other properties. The MCT project, designed as a software package capable to perform simulation and track reconstruction, utilizes the Athena framework, thereby benefiting from its flexibility and many other features. Reconstructed muon trajectories originating from data obtained by the measurement facility can then be used to do wire positions analyses.

Problems in the original MCT reconstruction processes highlighted issues which required further consideration. Additional, inner degrees of freedom in MDT chamber geometry lead to the necessity of delivering calibration algorithms which are able to determine further alignment parameters.

The MCT alignment process for the MDT chamber setup was changed and no longer makes use of data originating from the chamber which is to be tested. This was done in order to be independent of influences originating from possible distortions in the test chamber geometry. Alignment parameters for both global and inner alignment (that is, various multilayer and single-layer deviations from the nominal geometry, as well as different non-rigid-body distortions) are taken into account in the wire positions analysis. This software, formerly used just to calculate wire position deviations for each single tube, now additionally features algorithms to calculate intrinsic alignment parameters.

Extensive testing of established processes, together with implementations of new algorithms resulted in the means to do a calculation of the alignment parameters not only on a global, chamber-wide scale. The obtained results are in good agreement with X-ray tomography data from CERN.

Therefore, different effects in the MCT measurement and reconstruction processes, which required understanding are now taken into account and new tools have been developed to provide valuable calibration data for the ATLAS muon chambers.

Appendix A

Description of a MCT reconstruction job

Track reconstruction in this thesis was done by using the MCT package together with Athena version 6.3.0. Three processings of the raw data recorded by the Measurement facility have to be performed in order to calibrate and reconstruct muon trajectories. Two of them are calibration runs which address $T0$ -calibration and reference chamber alignment, as discussed in chapters 2.2.3 and 3.

The final step is to reconstruct event data in order to produce ROOT-N-Tuples containing track information. This job is started by

```
athena MCTNTuple_raw.txt
```

This command specifies a joboptions file to the application manager which specifies all algorithms and properties that are necessary for this particular process:

```
////////////////////////////////////
//
// MCTNTuple_raw.txt
// -----
//
////////////////////////////////////

#include "$ATHENACOMMONROOT/share/Atlas.UnixStandardJob.txt"
includes the Athena basic options that are mandatory for each reconstruction job

//-----
// configure application
//-----

ApplicationMgr.DLLs += { "GaudiAlg",
                        "GeoModelSvc",
                        "RootSvcModules",
                        "RootHistCnv",
```

```

"MuonCTDetDescr" ,
"MuonCTGeoModel" ,
"MuonCTIdentifier" ,
"MuonCTConditionsCnvSvc" ,
"MuonCTAlgs" ,
"MuonCTCalibAlgs" ,
"IOVSvc" ,
"MuonCTReco" ,
"MuonCTRecoUtils" ,
"MuonCTGraphics" };

```

Specify all run-time libraries that are needed.

```

ApplicationMgr.ExtSvc += { "AtRndmGenSvc" ,
"IOVSvc" ,
"IOVASCIIDbSvc" ,
"GeoModelSvc" ,
"MuonCTConditionsCnvSvc" ,
"TangentsOnCirclesSvc" };

```

Calls external services which are implemented in the libraries above.

```

ApplicationMgr.TopAlg = { "Sequencer/TopSequence" };

```

The application manager instantiates a Sequencer (which is a tool to organize algorithms), called "TopSequence" as the top algorithm.

```

TopSequence.Members = { "TDCDelayAdjust/TDCDelayAdjust" ,
"MDTTimeToRadTransform/MDTTimeToRadTransform" ,
"MDTPatternFinder/MDTPatternFinder" ,
"MDTTrackFitter/MDTTrackFitter" ,
"MuonCTNTuple/MuonCTNTuple" };

```

The configuration of "TopSequencer" is specified from Athena algorithms. Further information is given in chapter 2

```

MessageSvc.OutputLevel = 5; // 1=VERBOSE 2=DEBUG,
//3=INFO, 4=WARNING, 5=ERROR, 6=FATAL

```

```

MuonCTConditionsCnvSvc.OutputLevel = 1;

```

```

ApplicationMgr.EvtMax = 1000000;

```

Set different properties like standard output and maximum event numbers at run-time.

MsgSvc is set to an output level that produces only error messages on standard output.

Single sub-services can be manipulated in their output level as well.

```

// Pattern Finder

```

```

// -----

```

```

MDTPatternFinder.MinPerChamber = 5;

```

```

MDTPatternFinder.RoadWidth = 5.;

```

```

MDTPatternFinder.GlobalDeltaInter= 40.;

```

```

MDTPatternFinder.GlobalDeltaSlope= 0.2;

```

```

MDTPatternFinder.MaxResidualSum = 10.0;

```

```

MDTPatternFinder.MaxResidualAvg = 2.0;
MDTPatternFinder.GlobalPatternIgnoresMiddleChambers = true;
Further properties concerning pattern finding processes. Here, at least 5 hits are re-
quired to form a hit pattern and the test chamber is excluded from local pattern finding.

// Track Fitter
// -----
MDTTrackFitter.TrackFitter = "StraightLineDCFitter";
MDTTrackFitter.StraightLineDCFitter.LineDCFitter =
"MinuitDCLineFitter";
//-> from fastprod:
MDTTrackFitter.MinGlobalProb = 0.005;
Specify the track fitting strategy and the actual algorithm in MCT. "StraightLineDC-
Fitter" denotes fitting strategies using drift circles (DC, in contrast to track points,
TP) to perform line fits while "MinuitDCLineFitter" is the fit algorithm which utilizes
the MINUIT package to do the actual minimization.

// TrackFitMonitor
// -----
TrackFitMonitor.TrackFitterName = "MDTTrackFitter";

// GeoModelSvc
// -----
GeoModelSvc.Detectors = { "MuonCTIdHelperTool",
                          "MuonCosmicTeststandTool",
                          "MuonCTDetDescrTool",
                          "MCTCondMgrTool" };
Instantiate the Athena GeoModel. Different types of objects are stored in the detector
store as well as some other objects that are not related to the geometry description,
like "MuonCTIdHelperTool"

// Conditions
// -----
EventPersistencySvc.CnvServices += { "MuonCTConditionsCnvSvc" };
Activate the conditions conversion service.

ProxyProviderSvc.ProviderNames += { "IOVASCIIDbSvc" };
IOVASCIIDbSvc.DBname = "IOVDB";
IOVASCIIDbSvc.ClassID = { 4143, 4144 };
IOVASCIIDbSvc.UseDefaultRange = false;
Instantiate the IOVDB service. The root directory of the ASCII database is specified
as a local path here, as well as ClassIDs which are to be taken into account. The class
IDs specified here concern the calibration information regarding T0-Fits and chamber
alignment. A default range can also be used if there is no entry in the Interval of
Validity Database.

```

```
MuonCTConditionsCnvSvc.CondDBRoot = "CondDB";
```

Specify the root directory of the conditions database.

```
// RawData / MonteCarlo
```

```
// -----
```

```
//#include "MCTAthenaRootReadOptions.txt"
```

```
#include "MCTRawDataReadOptions_generated.txt"
```

Include a further file which contains information about the data to be processed.

```
// Histogramming, NTupleSvc
```

```
// -----
```

```
ApplicationMgr.HistogramPersistency = "ROOT";
```

```
HistogramPersistencySvc.OutputFile = "DigitMonitor.root";
```

```
NTupleSvc.Output = { "MuonCT DATAFILE='NTuples/MCTNTuple.root'
                    TYP='ROOT' OPT='NEW' " };
```

Specify ROOT N-Tuple output. This file contains the resulting track parameters calculated for each event.

```
// DumpDigits
```

```
// -----
```

```
DumpDigits.DumpMDTDigits = true;
```

```
DumpDigits.DumpScintiDigits = true;
```

```
DumpDigits.DumpStreamerDigits = true;
```

Print out digit information

```
// TDCDelayAdjust
```

```
// -----
```

```
TDCDelayAdjust.DebugHistograms = false;
```

```
//TDCDelayAdjust.DebugHistoOffset = 1100;
```

Digit histogramming properties

```
////////////////////////////////////
```

This Athena job writes a ROOT N-Tuple which contains track information about muon events. The ROOT-N-Tuple-file is the basis for the wire positions analysis.

Appendix B

Implementation of the new wire positions analysis

In order to address the issues concerning the determination of further alignment parameters, the original wire position analysis software was re-implemented. Keeping compliance with the Athena framework in mind, the code was put onto a C++ class frame, although it was not fully integrated into the MCT package, since some of the interface issues in Athena are not yet resolved in everybody's contentment.

The ROOT N-Tuple readout was re-used, as well as basic event-loop-algorithms. The fit procedures which determine the y and z wire position deviations utilize the robust-least-squares-fit method (see chapter 3.1.3) in order to get correct results for single wire displacements. Together with extensive histogram and console output functionality, the analysis software grew to about 3000 lines of code.

Using a separate `main()`-routine, the class, implemented as `NTupleAnalysis`, is instantiated and used there by calling the respective member functions. The work-flow of wire displacement determination, utilizing `NTupleAnalysis`, is depicted in figure B.1.

The results of displacement fits performed for the test chamber are filled into STL maps

- `std::map<int, double> front_y_displacements`
- `std::map<int, double> front_z_displacements`
- `std::map<int, double> back_y_displacements`
- `std::map<int, double> back_z_displacements`

which are declared as private data members and connect wire numbers with their displacement values. Therefore, every member function has access to these displacement maps and can read and correct specific wire deviations by referencing the respective tube number.

Subsequent steps address the determination of alignment parameters on different levels, as discussed in chapter 4. The member function `testChamberGlobalCorrections()` calculates the global alignment parameters ΔY , ΔZ , β and γ and corrects the displacement maps for these values.

The remaining parameter α is determined by separate member functions. Two options, `testChamberXAxisRotationCorrection()` and `testChamberXAxisRotationCorrectionfrontback()` exist. The former function is restricted to a global rigid-body-assumption and calculates a mean alignment angle α , while the latter function can be chosen in order to take twisted chamber ends into account. α is calculated and corrected separately for each chamber end.

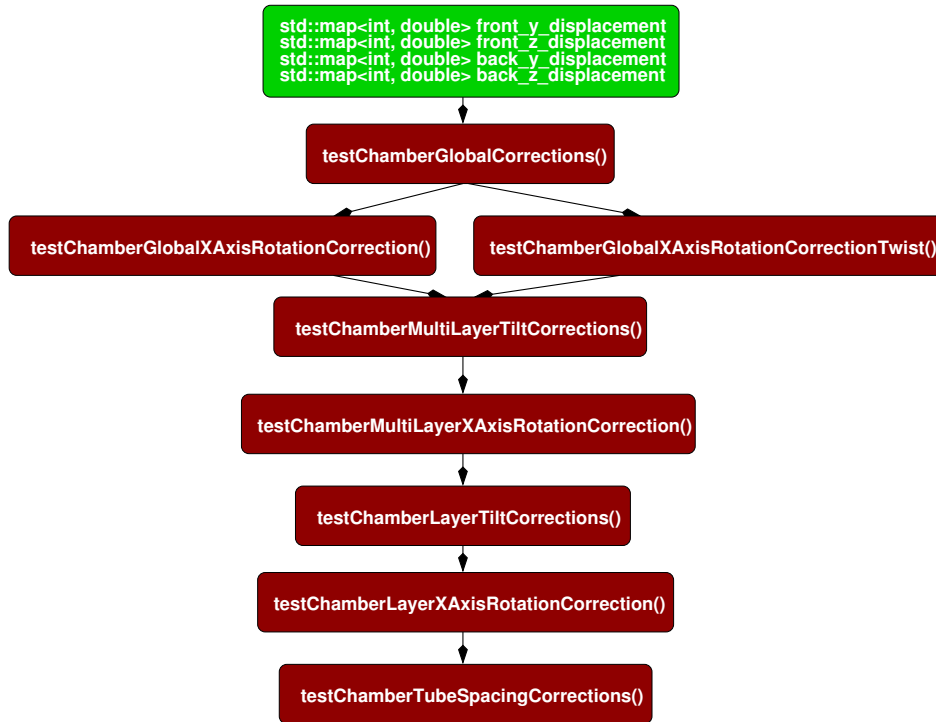


Figure B.1: Work-flow of the wire displacement determination software, with variables and methods described in the text. Methods for a global x-axis correction can be interchanged, depending on whether a correction for twisted chamber ends should be performed or not.

Further levels of alignment parameter determination and correction are implemented in

- `testChamberMultiLayerTiltcorrections()`
- `testChamberMultiLayerXAxisCorrection()`
- `testChamberLayerTiltCorrections()`
- `testChamberLayerXAxisCorrection()`

These functions utilize similar proceedings as in global correction algorithms. Subsets of the displacement maps are identified and divided in multilayers or layers in order to determine separate alignment parameters for these elements.

The remaining tubespacing effects are taken into account in `testChamberTubespacingCorrections`. By again deriving subsets of wire displacement information from the STL maps, each single layer is addressed on both front end and back end, thereby calculating separate tubespacing parameters.

Bibliography

- [1] *ATLAS Detector And Physics Performance*, CERN/LHCC 99-14
- [2] *ATLAS posters*,
<http://atlas.web.cern.ch/Atlas/documentation/poster/HTML/>
- [3] *R.Brun, F.Rademakers, ROOT System Homepage*, <http://root.cern.ch>
- [4] *The Gaudi Collaboration*, <http://proj-gaudi.web.cern.ch>
- [5] *The Geant4 Collaboration*, <http://cern.ch/geant4/>
- [6] *Athena User Guide and Tutorial*, CERN, 2003
- [7] *Athena Developer Guide*, CERN, 2004
- [8] *ATLAS C++ Coding Standard Specification*, CERN, 2003
- [9] *CLHEP - A Class Library For High Energy Physics*,
<http://wwwinfo.cern.ch/asd/lhc++/clhep/>
- [10] *H.van der Graaf, H.Groenstege, F.Linde, P.Rewiersma, RasNiK, an Alignment System for the ATLAS MDT Barrel Muon Chambers - Technical System Description*,
NIKHEF/ET38110, 2000
- [11] *V.Blobel, Tracking methods overview, HERMES meeting, Zeuthen 2003*
<http://www.desy.de/blobel/phystat.html>
- [12] *MPI MDT assembly page*,
http://www.atlas.mppmu.mpg.de/atlas_mdt/subpages/mdt_wire.html
- [13] *O.Biebel et al., A Cosmic Ray Measurement Facility for ATLAS Muon Chambers*,
arXiv:physics/0307147, LMU-ETP-2003-01
- [14] *A.Brandt, Simulation and Reconstruction of Muons at the Munich ATLAS Cosmic Test Facility with Athena*,
LMU, 2003
- [15] *A.Brandt, G.Duckeck, P.Schieferdecker, MuonCosmicTeststand source tree via US ATLAS LXR-Code Browser*,
<http://atlassw1.phy.bnl.gov/lxr/source/atlas/MuonSpectrometer/MuonCosmicTeststand/>

- [16] *O.Kortner, Schauerproduktion durch hochenergetische Myonen und Aufbau eines Höhenstrahlprüfstands für hochauflösende ATLAS Myonkammern*, Doctoral Thesis, LMU Munich, 2002

- [17] *F.Rauscher, Test von Driftkammern mit kosmischen Myonen: Bau der ersten Ausbaustufe des Teleskops und Untersuchung seiner Leistungsfähigkeit*, LMU Munich, 2001

Vielen Dank an...

- ...Prof. Dr. Dorothee Schaile für ihr uneingeschränktes Verständnis und Rücksichtnahme auf meine Situation
- ...Prof. Dr. Wolfgang Dünneberger für die Erstellung des Zweitgutachtens
- ...Günter Duckeck für seine Geduld mit mir und für die erstklassige Betreuung meiner Diplomarbeit
- ...John Kennedy für das Korrekturlesen meiner Arbeit
- ...Felix Rauscher für wertvolle Informationen über den Meßaufbau und zu programmiertechnischen Problemen
- ...Prof. Dr. Ottmar Biebel für neue physikalische Einsichten in diversen Diskussionen und für seinen Rat bei verschiedensten Problemen
- ...Marion Erlebach für ihren Zuspruch in hektischen Zeiten und für ihre wertvolle Hilfe bei der optischen Gestaltung der Arbeit
- ...Matthias Schott für die gute Nachbarschaft und angenehme Büroatmosphäre
- ...Johannes Elmsheuser, Tim Christiansen und Fritz Vollmer für sehr viele kleine und größere Tips
- ...allen Angehörigen des Lehrstuhls für das hervorragende Klima: Prof. Dr. Arnold Staude, Herta Franz, Meta Binder, Philippe Calfayan, Jörg Dubbert, Frank Fiedler, Alexander Grohsjean, Tatjana Kennedy, Petra Haefner, Ralf Hertenberger, Britta Leonhardt, Raphael Mameghani, Doris Merkl, Thomas Nunnemann, Philipp Schieferdecker, Raimund Ströhmer und Attila Varga.
- ...meine Eltern, ganz besonders meine Mutter, die mich immer vorbehaltlos unterstützt hat

Selbstständigkeitserklärung

Ich versichere hiermit, die vorliegende Arbeit selbstständig verfasst zu haben und keine anderen als die angegebenen Quellen und Hilfsmittel verwendet zu haben.

Matthias Obermaier

München, 28. Januar 2005

